

18. 03. 83

• La Silla
• La Serena
• Santiago

EL MENSAJERO



ESO

No. 31 – March 1983

46 86

Latest News about the European Coordinating Facility for the Space Telescope

On the 23rd of February, a Memorandum of Agreement concerning the European Coordinating Facility for the Space Telescope was signed in Paris by the Director General of the European Space Agency (ESA), Mr. E. Quistgaard, and the Director General of the European Southern Observatory, Prof. L. Woltjer. The ceremony took place in the presence of the members of the ESA Council.

The aim of the agreement is to define the modalities of the cooperation between ESA and ESO for the operation of the ST/ECF, which will be established as a separate unit at ESO in Garching. The prime purpose of the establishment of the ST/ECF is to enhance the capabilities within Europe for the

scientific use of the Space Telescope and of the Space Telescope data archive.

To achieve this aim, the ST/ECF shall provide a convenient source of detailed knowledge in Europe of the Space Telescope and its associated instruments, ensure coordination of software developments for ST within Europe and with the ST Science Institute in the U.S., and contribute to the archiving, cataloguing and disseminating of ST data to European scientists. ESA and ESO will each provide seven persons towards the staffing of the ST/ECF. ESO will have the primary responsibility for the day-to-day functioning of the ST/ECF. It is expected that the ST/ECF will begin functioning in a limited way later this year.

Fiber Optics at ESO

Part I: Coupling of the CES with the 3.6 m Telescope Using a 40 m Fiber Link

D. Enard and G. Lund, ESO

During an experimental run made in November 1982, two entirely different and independent fiber optic systems were tested at the 3.6 m telescope. In the present article, a description is given of the first, which consisted essentially of an optical fiber link between the 3.6 m prime focus and the CES input slit.

In the next issue of the Messenger, the multiple-object fiber-spectroscopy system will be described.

Technical Description

The purpose of this project was to determine the usefulness of a long single fiber link between the 3.6 m prime focus and the CES spectrograph using a suitable adaptation of the output beam divergence together with an image slicer.

The essential components developed for this project were: the fiber link with its end connectors, the mechanical and optical guiding elements, provision for illuminating the fiber with calibration lamps, and the output beam optics coupled with an image slicer. A brief description of the above components is provided in the following paragraphs:

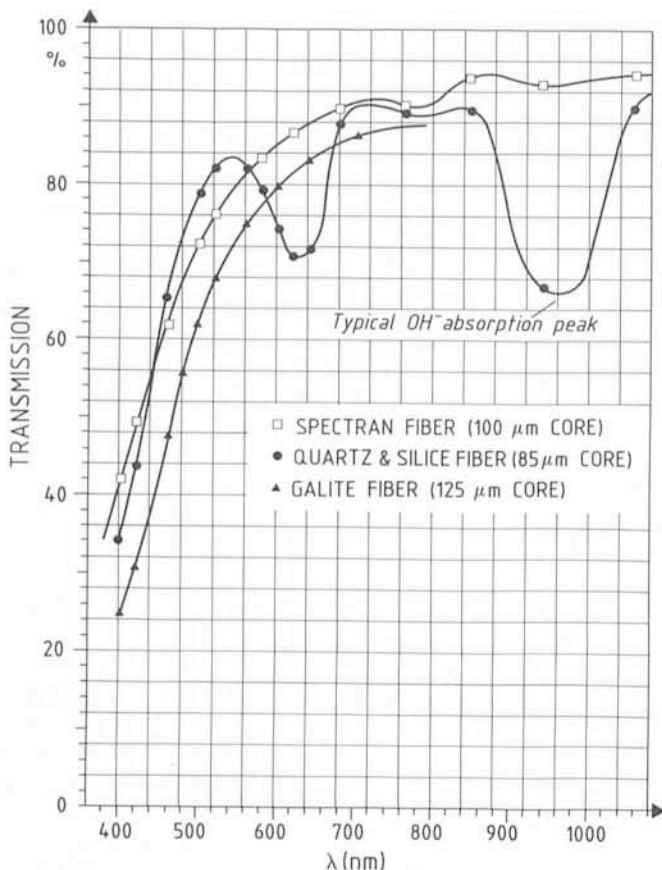


Fig. 1: Spectral efficiency of the three 40 metre fiber optics cables. Considerable attenuation at blue wavelengths is evident in all three fibers, although a useful spectral range from 5000 Å to 1 μm is available. (Most commercial fibers are optimized at 0.85 μm or 1.3 μm for telecommunications applications). All measurements were made at f/2.8.

1. Fiber Link

Three different optical fibers (each roughly 38 m long and housed in a protective cable) were prepared for this experimental run. They were distinguished mainly by their core diameters (85 μ, 100 μ and 125 μ) and to a certain extent by their laboratory measured spectral transmission (Fig. 1) and their output beam divergence. Both ends of each fiber were mounted in a specially developed ESO connector. As shown in Fig. 2, the fiber input end was covered by an inclined diaphragm whose rear surface acts as a mirror except for a hole slightly larger than the fiber core. An oil immersion was employed to ensure satisfactory optical matching between the fiber and diaphragm.

At the output end of the link a similar connector was used to accurately align the fiber with a beam focussing system. An immersion oil was used between fiber and lens for correct optical matching.

2. Acquisition, Guiding and the Prime Focus Adaptor

When correctly aligned in the primary focal plane, the image of the star of interest is focussed onto the fiber input end, as illustrated in Fig. 2. The principle of the prime focus adaptor, designed for ease of acquisition and guiding, is illustrated in Fig. 3; for the purpose of initial acquisition the mechanical support, holding together the prism-lens assembly (used for calibration) and the acquisition mirror, is swung in front of the incident beam permitting the star of interest to be found within a field of roughly 6' × 6'. At the same time either of the calibra-

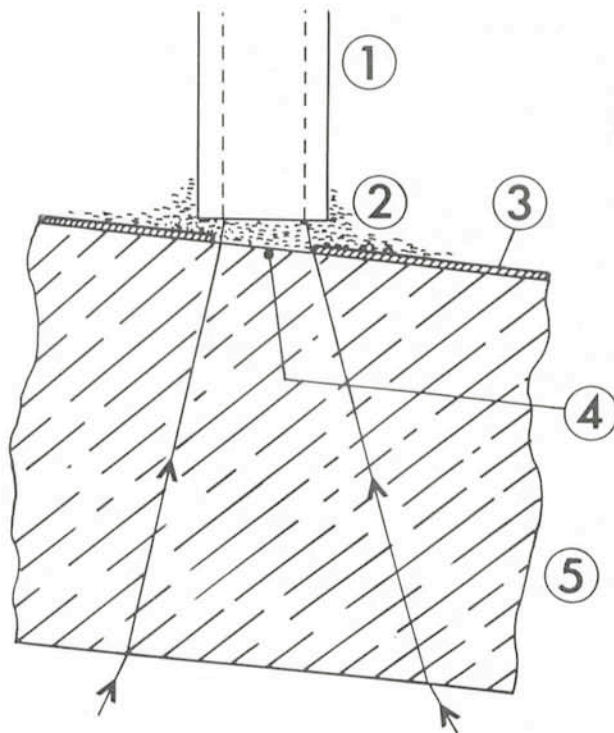


Fig. 2: Schematic view of the fiber input-inclined diaphragm assembly. This design enables the focussed star image to fall, via a hole in the mirrored diaphragm, onto the input end of the fiber. Any coronal residual of the image is viewed at the edges of the hole via a TV camera. The numbered components are: 1. Optical fiber; 2. Immersion liquid; 3. Aluminized surface; 4. Non-Aluminized hole; 5. Silica cover plate.

tion lamps may be switched on for determining the spectral calibration and flat-field response of the spectrograph. The lamp beams are focussed onto the fiber end via the prism lens arrangement.

In order to center the star accurately onto the fiber, the prism-mirror assembly is swung out of the telescope beam, thus allowing reflected light from the fiber diaphragm to be re-imaged with a magnification factor ~ 3 (via lens triplet 2, mirror 2 and mirror 3) onto the TV camera. In this mode, since the fiber diaphragm is aluminized except for a hole aligned with the fiber

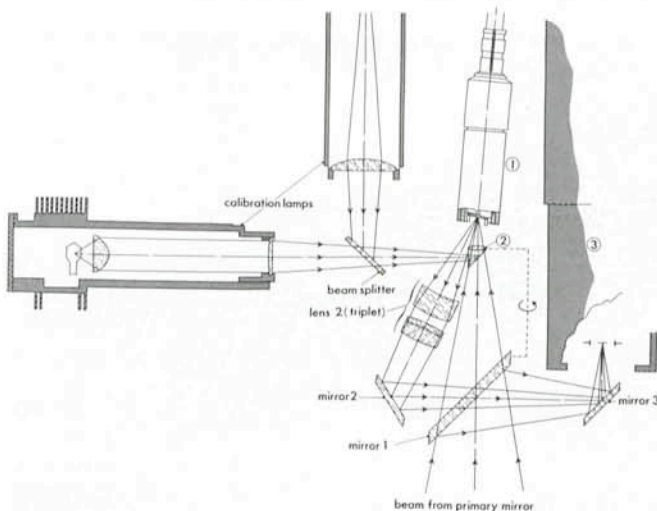


Fig. 3: Schematic view of the adaptor-guiding unit. This assembly is installed at the prime focus of the 3.6 m telescope. Essential elements not described in the figure are: 1. ESO connector and diaphragm assembly (Fig. 2); 2. Calibration prism-lens assembly; 3. High-gain TV camera.

core, the correctly guided star is observed as a "black hole" surrounded by a bright corona whose extent depends upon the TV camera gain and the actual seeing conditions. At a later date, an autoguiding system could be used directly with this TV image.

3. Output beam optics

The $f/3$ prime focus input beam profile is transferred through the fiber almost undisturbed, with only a few per cent of the input energy being scattered beyond the nominal $f/3$ beam (Fig. 4).

A cemented triplet objective produces a $10\times$ magnified image of the fiber output end at the entrance slit of the spectrograph, thus reducing the beam aperture to $f/30$ which is then compatible with the spectrograph optics.

If a certain degradation in resolution can be tolerated, the normal CES input slit can be used at a wide setting so that most of the light enters the instrument. If the condition of maximal resolution is determinant for a particular observation, this slit can be replaced by an image slicer. The image slicer used during the test period was designed by H. Richardson (E. Richardson, "Image Slicers for Image-Tube Spectrographs", ESO/CERN Conference on Auxiliary Instrumentation for Large Telescopes, May 2-5, 1972, p. 275), and is essentially an image anamorphoser comprising an input cylindrical lens, an input slit, two split offset spherical mirrors and an output slit. If considered as a black box, the slicer can be thought of as allowing one direct slice of the image through the exit slit, and placing above and below this slice one (or more) slice(s) taken from each of the two remaining (and otherwise lost) crescent-shaped edges of the image. Higher order slices are also present but are not made use of in this design because of the limited diode length of the reticon. This system, if well adjusted, provides a theoretical gain of around 2.5 for an exit slit width of $230\ \mu$ and a uniformly illuminated fiber end $85\ \mu$ in diameter. Such a configuration is of course only useful if the detector pixels are sufficiently dimensioned (as is the case with the CES reticon for up to 3 slices) to make use of the elongated entrance slit spectrum.

Test Results

The 3 cabled fibers prepared for this experiment were installed on the telescope in less than a day. They were fed down through the prime focus via the Serrurier structure and one of the coudé tubes into the coudé room.

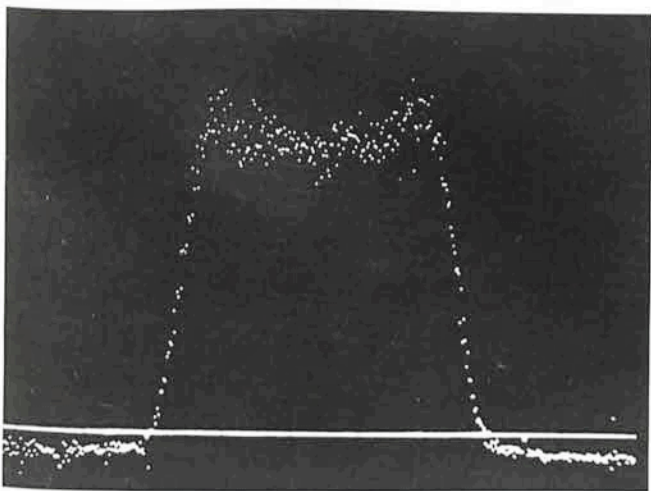


Fig. 4: Output beam profile of the fiber. This profile was obtained with the complete fiber link and a bright star. A reticon was set at a certain distance from the fiber end and used to record the angular distribution of light at the fiber output. Calculations show that more than 95 % of the energy in this beam is admitted into an $f/3$ optical system.

Tentative Time-table of Council Sessions and Committee Meetings in 1983

April 6-8	Committee of Council (Chile)
May 3-4	Finance Committee
May 5	Users Committee
May 20	Scientific and Technical Committee (Cargèse, Corsica)
June 6	Council (Observatoire de Haute-Provence)
June 8-9	Observing Programmes Committee
November 8	Scientific and Technical Committee
November 9-10	Finance Committee
November 11	Committee of Council
November 29-30	Observing Programmes Committee
December 1-2	Council

All meetings will take place at ESO in Garching unless stated otherwise.

Fig. 1 clearly illustrates that the present fibers cannot be used efficiently in the blue over relatively long distances and for this reason no attempt was made to work in this spectral region. Most of the observations were made at wavelengths greater than $5600\ \text{\AA}$. The adapter and guiding unit developed for the prime focus were found to be totally satisfactory: star acquisition and guiding with the TV camera was extremely easy and the calibrations obtained through the fibers led to integration times equivalent to those necessary with the spectrograph calibration system. Although no adequate comparison has yet been performed, it is expected that calibrations achieved via an optical fiber should give improved overall accuracy.

1. Fiber Efficiency

Efficiency comparisons using different combinations of fiber and slit (or image slicer) were handicapped by the extreme sensitivity of the system to seeing. This is unfortunately a parameter which, by its own nature, evolves quite rapidly and unpredictably.

From the tests performed over 3 nights it seems that 2 of the fibers (Quartz and Silice $85\ \mu\text{m}$ diameter and Galite $125\ \mu\text{m}$) gave comparable results whereas the $100\ \mu\text{m}$ fiber, which in the laboratory exhibited considerable aperture degradation, was found to be inferior. The similarity in results obtained with the $85\ \mu\text{m}$ and $125\ \mu\text{m}$ fibers can be explained by the fact that although the former has a smaller collecting area, this drawback is compensated for by a superior matching of output image to entrance slit size.

2. Image Slicer Performance

The efficiency of the image slicer was measured by comparing its throughput with that obtained with a conventional slit of the same width. The gain was in this case found to be about 2, whereas a factor of 3 to 4 (depending on fiber diameter and seeing) was achieved with no image slicer by opening the spectrograph slit sufficiently to accommodate the projected image of the fiber output. This result stresses the extreme dependence of the overall system efficiency upon seeing and image slicer efficiency.

3. Astronomical Results

During the last test night, the relatively faint LMC star HD 269700 was observed (Fig. 5). This star has a magnitude of 10.54, and was observed with the $85\ \mu\text{m}$ fiber together with a

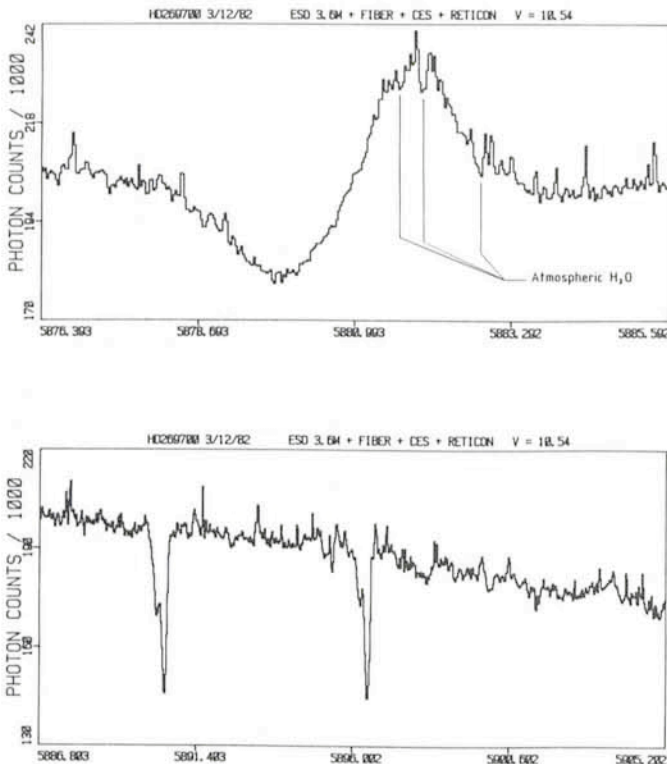


Fig. 5: Reticon spectrum of the LMC star HD 269700 ($M_v = 10.54$). This spectrum was obtained after 3.5 hours of integration using the 3.6 m telescope and a 85 μm core fiber.

(a): the P Cygni profile of He I. The detected emission and absorption line velocities are respectively 320.76 and 216.5 km sec^{-1} .

(b): Na I interstellar absorption lines. The two deep lines are galactic components, whereas several other fainter components associated with the LMC itself can also be detected.

large slit; the resolution was thus degraded by a factor of about 3 to a value of 160 $\text{m}\text{\AA}$ (FWHM). The seeing during this observation was excellent, and possibly as much as 80 % of the light was captured by the fiber. The signal to noise ratio was about 100 and the gain compared with similar observations with the CAT corresponds to about 2 magnitudes, equivalent to the ratio of the collecting areas of the 2 telescopes. This stresses the important result that the fiber link itself can, under certain conditions, be extremely efficient and that the 2 main

sources of loss are those due to input coupling with the telescope (limited by the seeing) and those due to coupling with the spectrograph (limited by the slit width).

Conclusions

It has been demonstrated that a fiber optics link could be used efficiently to couple an instrument to a telescope over distances of several tens of metres. The coupling efficiency is limited by two conflicting requirements: a large fiber should be used for good compatibility with the average seeing disk, whereas considerations of optimal slit matching would require a smaller fiber to be used.

Because of its circular collecting area, the fiber is more sensitive to seeing degradation than a normal spectrograph slit. For this reason, the potential efficiency of future systems will be to a large extent dependent upon the development of an image slicer capable of efficiently ($\sim 100\%$) anamorphizing the output light distribution into a form entirely compatible with the spectrograph input requirements. Such an image slicer would then permit much larger fibers (limited in diameter only by the useable entrance slit or detector length) to be envisaged, thus significantly reducing the seeing dependence. This problem is not only relevant to the particular case of the CES, but is also of prominent interest for the development of future very large telescopes for which the instrumental coupling efficiency will be a critical parameter.

Before long a CCD will be installed on the CES and the present limitation in detector length will disappear, enabling a larger fiber diameter and consequently higher slicing factor to be implemented.

This new detector, when used together with an improved image slicer and fiber optics link, will yield a gain of 3 to 4 magnitudes at the 3.6 m telescope when compared with the present CAT/RETICON configuration.

It is hoped that within the first half of 1984, a fully operational and optimized fiber optics link will be ready for routine use by astronomers.

Acknowledgements

The recent experimental run made at La Silla was made possible only by the active cooperation of many staff members of ESO (at Garching and La Silla). In particular, we would like to thank S. Balon, B. Buzzoni, R. Ferlet, G. Huster, J. L. Lizon and E. Maurice for their respective contributions.

ESO Workshop on "Primordial Helium"

Some 60 participants attended a workshop on Primordial Helium and related light elements at Garching on February 2-3, 1983.

Theoreticians opened the workshop by stressing the importance of abundance measurements for the primordial elements. They outlined how recent developments in particle physics and cosmology have created great interest in determining accurate primordial abundances.

The various observational approaches to determining Y_p (the primordial helium abundance) were elaborated by many speakers. It was striking to see that from the smallest systems (planets, individual stars) to the largest (extragalactic HII regions) abundances could be obtained with reasonable accuracy. We heard about investigations of the Sun, the atmospheres of Jupiter and Saturn, and young and old stellar systems. Opposite viewpoints were expressed with respect to

prospects of obtaining accurate abundance determinations from globular clusters. Possibly the greatest controversy concerned approaches to Y_p using galactic and extragalactic HII regions - this involved observers, specialists in the interpretation of atomic spectra, and theorists of stellar and galactic evolution. New possibilities were investigated, involving supernova remnants, active galactic nuclei, and absorption lines in QSO spectra.

Reviews of the latest results concerning other light elements were also given - deuterium, lithium-7 and helium-3. These were considered, together with the best estimates of Y_p , in a very lively discussion session at the end of the workshop, and theoreticians elaborated their views on the status of the standard Big-Bang Cosmology and explored alternatives.

The proceedings of the workshop will be published by ESO within a few months.

P.A.S. and D.K.

The Galaxy NGC 1365

P. O. Lindblad, S. Jörsäter and A. Sandqvist, Stockholm Observatory

One of the most beautiful barred galaxies in the sky is found in the southern hemisphere, in the Fornax cluster at a declination of -36° . The galaxy – NGC 1365 – with its diameter of 11 arc minutes and its prominent spiral structure stands out well among the cluster galaxies. Situated 1.2 degrees from the cluster centre and with a radial velocity of $+1,650 \text{ km s}^{-1}$ – very close to the average radial velocity of the cluster – it is very probably a member. Among its closest neighbours we find the peculiar radio galaxy Fornax A and NGC 1386, which is the nearest type 2 Seyfert galaxy known.

NGC 1365 was one of the first galaxies to be photographed with the ESO 3.6 m telescope by Svend Laustsen and Hans Emil Schuster during the commissioning phase, and it was observed by one of us (P.O.L.) during the first visiting observers run with the 3.6 m telescope in October 1977. Two plates from this observing run are seen as Figs. 1 and 2.

As can be seen in the two-hour exposure the bar and spiral arms are prominent – the latter delineated by bright H II regions. There are strong absorption lanes along the bar and the spiral arms, as well as an intricate pattern of dust lanes and bright branches and twigs. In particular, there is a set of dark whisps across the bar extending from (or rather running into) the prominent absorptions on the front side of the bar.

If we estimate the distance of the Fornax cluster to 20 Mpc, the diameter of NGC 1365 as seen in Fig. 1 is 65 kpc and the total absolute magnitude -21.6 , i.e. it is a true supergiant galaxy. Spectral data show that the NE side is approaching and the SW side receding. If the spiral arms are trailing, then the NW side is the near one. With its inclination of 55° to the plane of the sky and a position angle of the bar 35° from that of the minor axis the orientation of the galaxy is very well suited for dynamical studies.

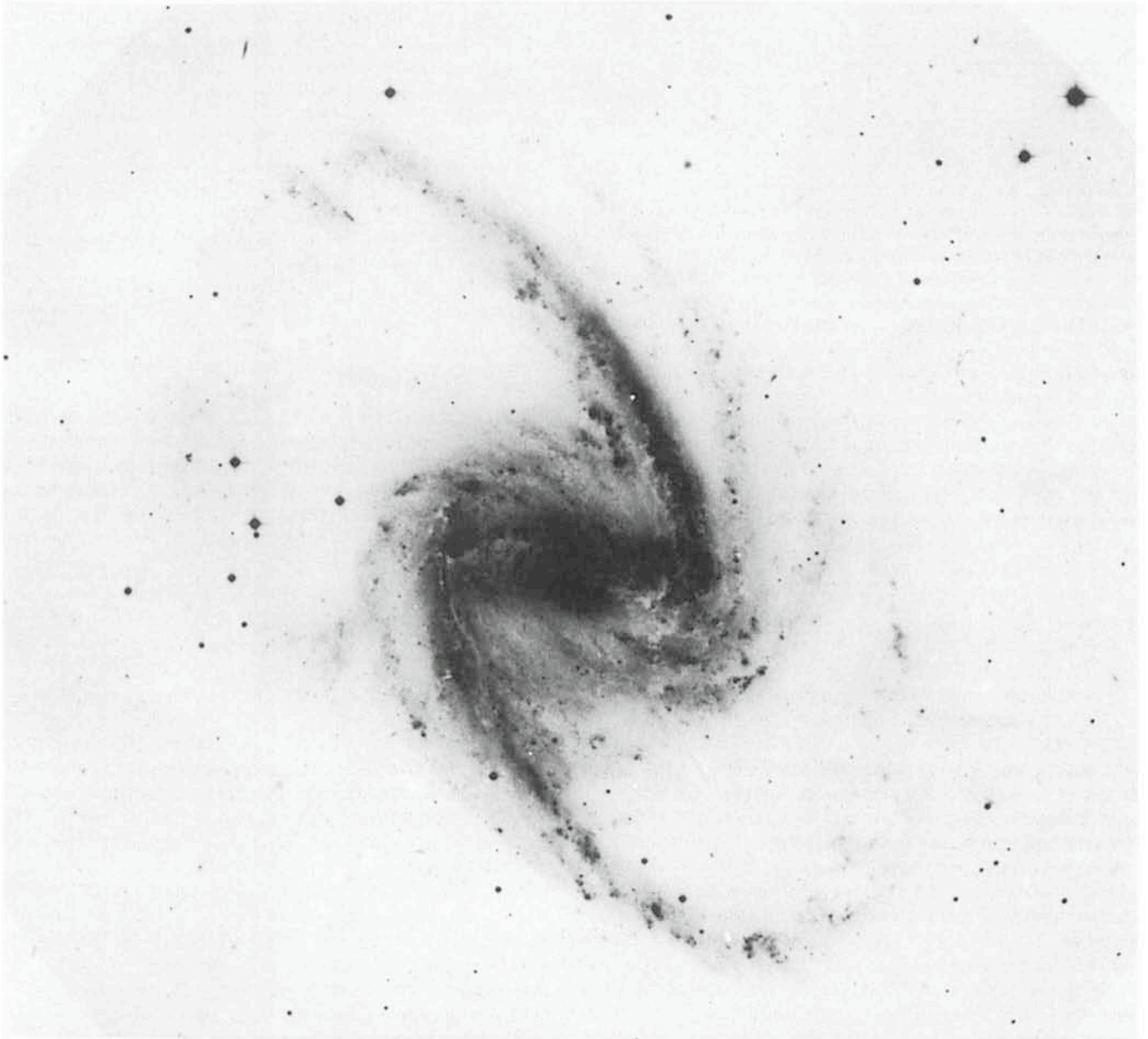


Fig. 1: ESO 3.6 m photograph of NGC 1365 obtained in a two-hour exposure on a III a–J plate with GG 385 filter.

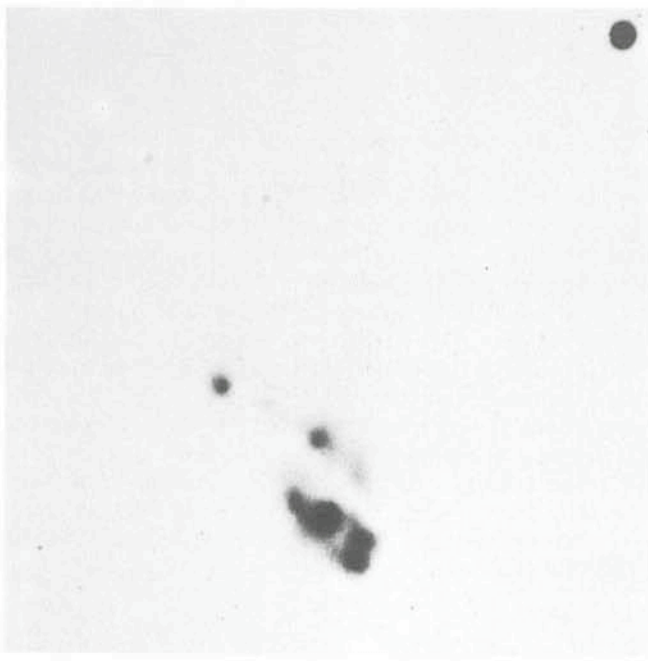


Fig. 2: ESO 3.6 m photograph of the nucleus of NGC 1365 obtained in a one-hour exposure on a 127-04 plate with narrow-band $H\alpha$ filter.

Since the middle of the 1970s the dynamics of barred galaxies has been intensely studied from a theoretical point of view as it has been realized that the stability of bars made up of stars and their perturbing influence on gas flow are fundamental keys to the understanding of spiral structure in galaxies. Numerical n-body calculations have shown that stellar systems of sufficient angular momentum are highly apt to form bars that are very stable. Numerical gas flow calculations have shown how a bar potential can create large-scale shocks along the bar as well as a spiral structure in the region outside the bar. On the other hand, observational confirmation of the predicted kinematics has been rather scarce. This is due partly to the slow process by which an extragalactic object can be covered with slit spectra, the low angular resolution of radio telescopes and, in particular, the lack of neutral or ionized atomic hydrogen in the bar region. NGC 1365 was chosen for studies with the 3.6 m telescope, because of its ideal orientation for kinematic studies, its clean structure and richness of interstellar matter, and, not least, because early observations by the Burbidges at Mc Donald had shown that the strong emission line spectrum from the nuclear region might imply violent noncircular motions.

The nuclear region of NGC 1365 is penetrated by a strong dust lane and contains a number of so-called "hot spots" and H II regions, almost all situated along the nearer arm of a small nuclear spiral as seen in Fig. 2. The nucleus itself is much redder than the surrounding hot spots and shows a strong infrared excess. At least part of this redness is caused by the absorbing dust lane just touching the nucleus.

Already our first spectra of the nucleus showed that the $H\alpha$ line in emission was suspiciously broad. In our discussions at ESO this aroused the immediate interest of Philippe Véron. IDS spectra secured by him and later by Danielle Alloin and P.O.L. showed that the $H\alpha$ line contained a broad component with a full width at half maximum intensity of $1,700 \text{ km s}^{-1}$, while the forbidden lines remained unresolved at 4 \AA resolution. This revealed the Seyfert 1 character of the nucleus (*Astron. Astrophys.* **87**, 245, 1980; **101**, 377, 1981).

This nucleus is surrounded by a rapidly spinning narrow line disk with a radius of about $7''$ corresponding to 700 pc as is

clearly displayed by the inclined emission lines. The position angles of the maxima and minima of the velocity gradients coincide closely with the position angle of the line of nodes as given from faint outer isophotes of the two-hour exposure in Fig. 1. There is of course no need for the plane of the nuclear disk to have the same orientation as that of the outer edge, but we can state that the velocity gradients of the nuclear disk as given by the $H\alpha$ and [N II] lines give no reason to assume anything but circular rotation of this disk with an angular velocity of $280 \text{ km s}^{-1} \text{ kpc}^{-1}$, or about ten times the angular velocity of the sun around the galactic centre. This gives a mass for the nucleus of the order of 10^9 solar masses.

The velocity field outside the nuclear region has been measured from our slit spectra with the Boller & Chivens spectrograph on the ESO 3.6 m telescope equipped with image tube or with the Image-Photon-Counting System of Boksenberg, from image-tube slit spectra obtained by Charles Peterson with the 4 m telescope at Cerro Tololo, from TAURUS observations on the ESO 3.6 m and from 21 cm observations by J.M. van der Hulst with the VLA. All these velocity measurements are now in some stage of reduction. All of these observations have strong signals in the spiral arms, but all suffer from the weakness of the emission lines in the bar. Only the IPCS spectra contain absorption lines to give information about the stellar motions. A preliminary rotation curve based on Charles Peterson's and our spectra is shown in Fig. 3. The pattern of systematic deviations from this curve are studied and will be combined with photometry and numerical calculations carried out in Collaboration with Preben Grosbøl and E. Athanassoula.

As is well known from the observations of M51 by Mathewson, van der Kruit and Brouw, large-scale galactic shocks may reveal themselves by enhanced non-thermal continuum radio emission. Inspired by these beautiful results, we set out to observe NGC 1365 with the Very Large Array (VLA) in New Mexico. The resolution with this radio synthesis interferometer would be of the order of arcseconds and our hope was to detect enhanced continuum radio emission from the strong dust lanes along the bar and spiral arms, where the existence of galactic shocks could be expected.

The observations with the VLA were carried out at 6 and 20 cm wavelength in November 1979 (*Astron. Astrophys.* **110**, 336, 1982). At that time the VLA was not fully finished—in particular the northern arm was very short, which resulted in a rather elongated beam shape for this southern object. As a matter of fact NGC 1365 lies rather close to the southern limit

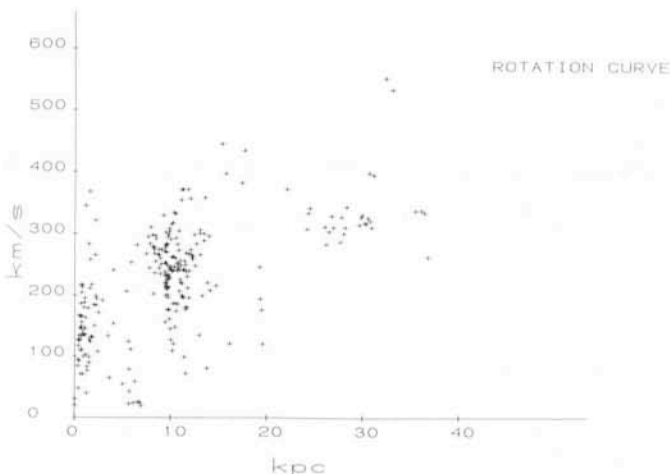


Fig. 3: Preliminary rotation curve of NGC 1365 derived from ESO 3.6 m Boller & Chivens spectra and spectra obtained by Charles Peterson with the 4 m telescope on Cerro Tololo.

for observations with the VLA and the integration time was maximized at 6 hours for each wavelength region.

As it turned out, however, there was no trace of a radio emission from the bar and the spiral arms, but the nuclear region again proved to be rather interesting. The highest resolution was reached at 6 cm, and Fig. 4 shows our 6 cm radio map superposed on the optical $H\alpha$ picture of the nuclear region. As can be seen, the radio structure is resolved into a number of components, some of which are still unresolved at arcsecond resolution. These discrete sources have intensities of 1–8 mJy. The total flux from the nuclear region is 190 and 450 mJy at 6 and 20 cm respectively. This gives an average spectral index of -0.72 which indicates non-thermal radiation and is a normal value for Seyfert galaxies. Observations with the Einstein satellite by T. Maccacaro, G.C. Perola and M. Elvis show that the soft X-ray luminosity is $1.6 \cdot 10^{41}$ erg s^{-1} (0.2–3.5 keV).

The intriguing question is now of course the nature of the radio sources and the optical hot spots, their interrelation and the origin of their energy output. As can be seen from Fig. 4, there is no clearcut correspondence between radio sources and optical hot spots, and the Seyfert nucleus itself is no strong source of radio radiation. Could activity in a Seyfert nuclear engine generate these compact sources far apart? But, at least as far as the $H\alpha$ and [N II] emission is concerned, there seems to be no clear evidence for violent outflow or drastically noncircular motion. Or could the radio sources be supernova remnants? The radio luminosity of each of the compact sources is of the order of 100 times CasA and their energy content can be modeled as if coming from 100 supernova remnants that would have to be confined to a volume of less than 50×200 pc. Steady-state calculations then show that about one supernova per year should occur in the nuclear region. So far, one supernova has been reported in 1957 to appear in one of the spiral arms. In the nuclear region a supernova would be more difficult to detect. As an alternative, one could imagine each compact source to be a radio supernova of the type detected in M 100, that reached a radio luminosity at 6 cm of 180 times CasA. Their life time, however, is only of the order of years and would cause a noticeable change of the radio emission over a short time. Our repeated 6 cm VLA observations in September 1982, although with lower resolution, give no evidence for such a variation.

To support the supernova rate mentioned each of the radio sources would have to be associated with about 10^5 O and B stars. This number of hot stars may not be inconsistent with the $H\beta$ flux from the hot spots that may be places for recent bursts of star formation. However, the luminosity function could not be

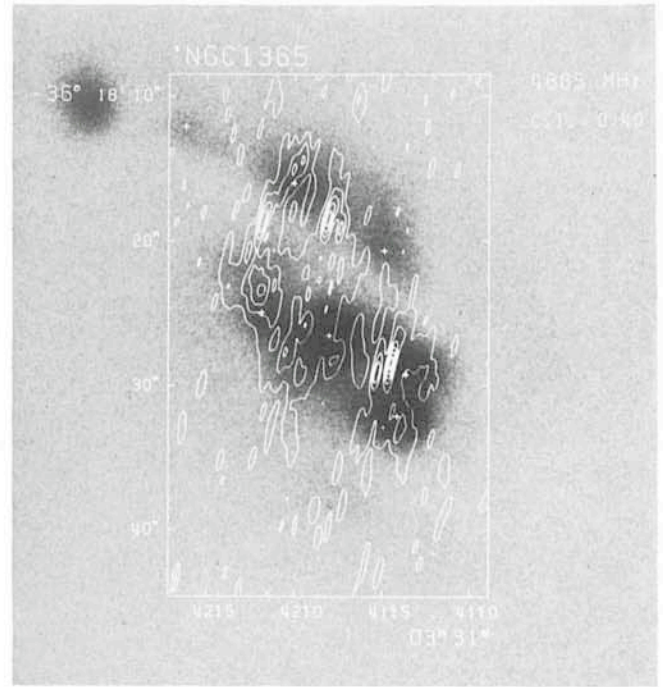


Fig. 4: The VLA 6 cm map superposed on the $H\alpha$ picture of Fig. 2.

a standard one, as the mass in low luminosity stars required would spoil the regular velocity field of the nuclear disk. Also the lack of clear association between concentrations of supernova remnants and hot stars needs an explanation.

In the midst of this puzzling situation a very important observation has appeared to add to the confusion, but not improbably to ultimately give the clue to what is going on. M.M. Phillips, A.J. Turtle, M.G. Edmunds and B.E.J. Pagel show in a recent preprint that extended regions of high-excitation gas around the nucleus reveal a velocity field considerably more complicated than the rotating disk inferred above from the $H\alpha$ and [N II] lines. As a matter of fact, the [O III] line at λ 5007 Å over this region is split up into several components with different velocities and velocity gradients. For some positions of their slit the [O III] line is actually inclined in opposite sense to that of the hydrogen lines. It seems that our IPCS observations show a peculiar behaviour also for the Ne III λ 3869 line. This may imply outflow of high-excitation matter from the nucleus in directions out of the plane of the disk. It could very possibly indicate a connection between the activity in the nucleus and the radio sources and hot spots in its surrounding.

Active Chromosphere in the Carbon Star TW Horologium

P. Bouchet, ESO, and M. Querci and F. Querci, Observatoire du Pic du Midi-Toulouse

Introduction

Herzberg (1948) was the first to suggest the existence of a corona-like nebulosity surrounding cool stars from strong Fe II emission lines he observed in the spectral region $\lambda\lambda$ 3150–3300 in the two supergiants α Herculis (M5 II) and α Scorpii (M1 Ib). Fifteen years later, Bidelman and Pyper (1963) suggested that these Fe II emission lines would be present in practically all giants of sufficiently late type. Then, Boesgaard and Boesgaard (1976) showed that this emission is nearly

universal in M-type stars and thus appears to be a natural occurrence in stars with low temperature. At present, these emission lines are recognized as an undisputed chromospheric indicator. Chromospheres have been detected in late-type (F–M) stars, in particular for M giants through their bright UV emission lines (the Fe II lines besides the Mg II h and k lines), and most notably Linsky (1980) has pointed out that a wider spectral range of stars than was thought previously may possess chromospheres.

Bidelman and Pyper (1963) reported for the first time ultraviolet Fe II emissions in the variable carbon star TX Psc, and suspected that the structure of the outer layers of C-type stars is not greatly dissimilar from that of M giants. However, in contrast with the detailed data available on the emission-line spectra of M-type stars, relatively little is known concerning the chromospheric emission lines in variables of the carbon class. In fact, as it was generally thought that high grain density in the atmospheres of the coolest low-gravity stars would prevent any manifestation of chromospheric emission lines, very few efforts have been made to determine the presence of these lines. However, recent observations are to be reported: in spite of the first, unsuccessful, attempts to record ultraviolet emission lines in the spectra of four cool carbon stars with the IUE satellite by Querci et al. (1982), positive results were obtained for other N-type stars by Johnson and O'Brien (1982) and by Querci and Querci (in preparation).

The observational confirmation of the presence of chromospheric emission lines in cool low-gravity stars is important to ascertain how the emission is related to the properties of the star, and to show what conditions favour the formation of the emission features. It is thus an important test of the validity of recent theoretical stellar-chromosphere models and their related heating mechanisms. Moreover, the study of a chromospheric activity in these stars may shed considerable light on the structure and dynamics of their outer layers about which very little is known. Estimates of the inner radius of the shell are not reliable, and consequently the mass loss rates are highly uncertain. The gas extension is not determined, and the possible asymmetries in the circumstellar lines which, for example, could result from the ejection of irregular masses, are only just beginning to be recognized, mainly due to recent

progress in echelle-resolution spectroscopy, as well as the possible polarization due to the envelopes themselves which are a mixture of gas and dust. Finally, and most important, it is difficult to understand the relation between the mass loss phenomenon and the stellar evolution. All the nonthermal mechanisms of mass loss are in themselves controversial.

Photometric and spectroscopic observations of a representative sample of C-type stars have been made mainly by one of us (P.B.) in the near-infrared, the visible and the near-ultraviolet. This sample was selected to cover a range of spectral types R and N, the latter including all types of variations (M, Lb, SRa, SRb) independently of the known existence or absence of a circumstellar shell. The observations were spread over several years in order to cover the phase of these stars over many periods of variability (from 150 to 500 days). In the sample of 12 stars, one, TW Hor (spectral type C7, 2 - NO), in fact a lot more observed than the others, showed (FeII) chromospheric activity with peculiar and surprising behaviour.

The Chromosphere of TW Hor

1. Spectroscopic Observations

Among the most important chromospheric spectroscopic indicators that can be detected in carbon stars, are the Ca II H ($\lambda 3968$) and K ($\lambda 3934$), the Mg II h ($\lambda 2803$) and k ($\lambda 2796$) lines and the Fe II lines around $\lambda 3270$. A search for Ca II and Fe II lines was made through observations with the coude spectrograph of the ESO 1.5 m telescope between 1979 and 1981. Conditions were the same for all spectrograms: 12 \AA mm^{-1} dispersion, Ila-O emulsion, 1" entrance slit and equal number

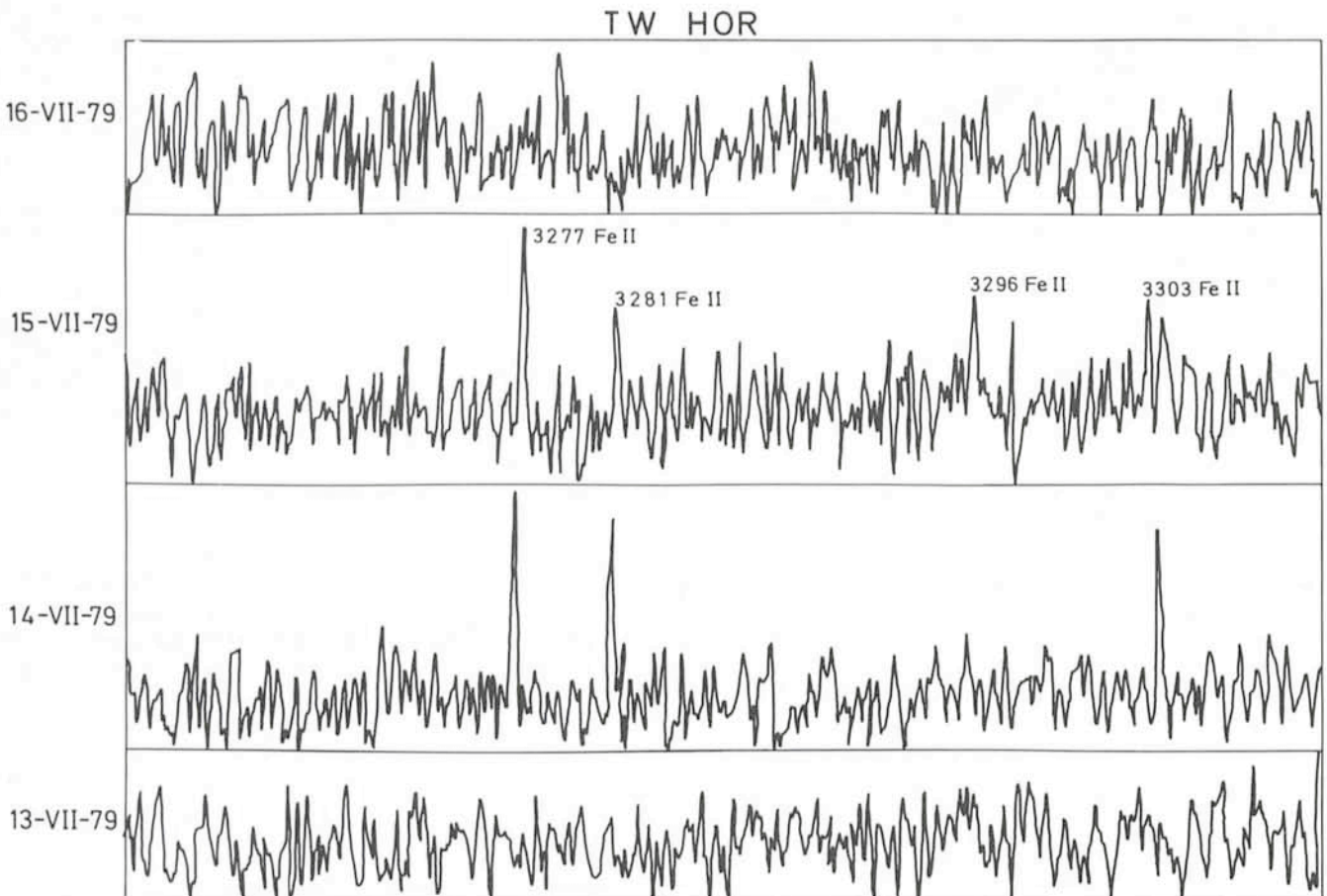


Fig. 1: Intensity tracings of plates obtained during four consecutive days in July 1979. No continuum is observed. Plates have been recorded at the CDCA (Nice Observatory) and processed at the Pic du Midi Observatory. (Ila-O emulsion, 12 \AA mm^{-1} .)

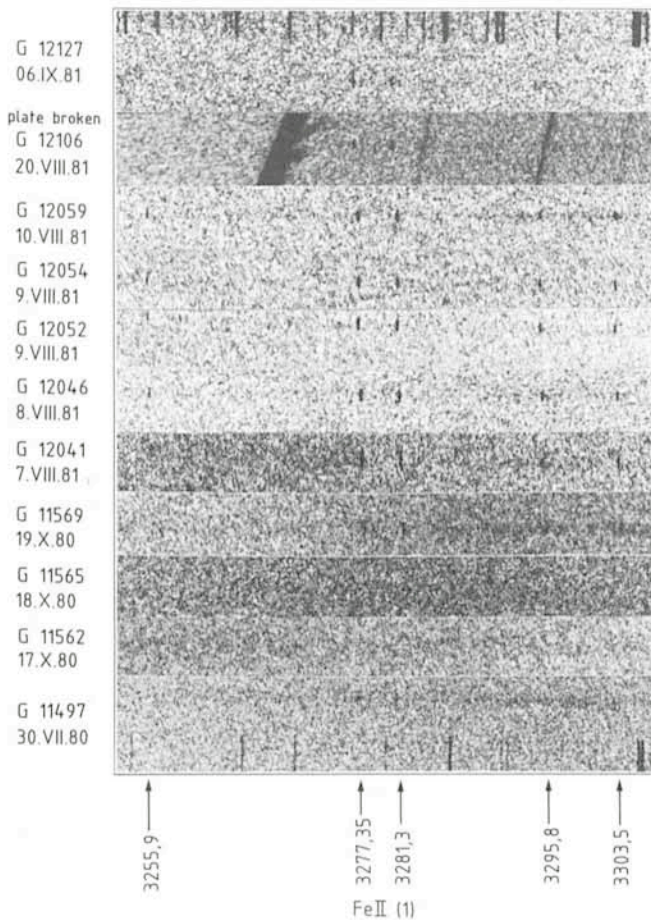


Fig. 2: A sample of spectrograms from July 1980 to October 1981. The two plates taken on August 9, 1981, (G 12052 and G 12054) are separated by 4 hours. Note that on plate G 12127 only the two strongest lines ($\lambda\lambda$ 3277, 3281) can be seen. Plate G 11497 has been exposed twice as long as the other ones. This photographic assembling was done by Mr. R. Donarski at La Silla. (IIa-O emulsion; 12 \AA mm^{-1}).

of counts from an exposure meter with a blue spectral response. In the spectral range $\lambda\lambda$ 3200–3500 the stars studied are so faint that in order to save exposure time, all spectra were taken without widening. However, due to faint continua, chromospheric lines, when present, stand out quite clearly. Figures 1 and 2 illustrate some results obtained for TW Hor. They show that the Fe II emission lines around λ 3270 vary in strength in an irregular manner and sometimes even disappear completely in time scales of one day.

Wide absorption profiles of Ca II lines have also been observed under the same conditions. Re-emission such as the one seen in K-type giants and in some R-type stars was not detected in TW Hor. Note that, even if such emission could be observed with better resolution and signal/noise, it would still be very weak.

Further to the observations made at La Silla, IUE spectra of TW Hor obtained in the LWR range, with low resolution and large aperture by Querci and Querci (in preparation) show a variable emission of the h and k Mg II lines, the C II] lines at 2325 Å, the Al III U2 and VII U7 lines, besides the UV Fe II lines.

2. Interpretation

The behaviour of the spectral lines, indicators of chromospheres as quoted above, has to be studied simultaneously in order to give an insight into the various possible excitation

mechanisms. In the case of TW Hor, a challenging point is that the Ca II H and K lines remain in absorption even when the UV Fe II and Mg II lines appear strongly in emission. It does not seem acceptable that the emission lines are excited in a shock front spreading across the photosphere, as generally accepted for Mira-type stars (for example, Hill and Willson, 1979): it would not explain why Ca II is never seen in emission, nor would it explain the irregular variations of the Fe II lines. Other possibilities can be considered, among which the following are the most outstanding:

A – There is a chromosphere which implies a permanent excitation of the Fe II lines. However, inhomogeneities of the cloud-like chromosphere layers may occasionally prevent detection of these lines. Short-term variability could be due to time evolution of active regions, or flares (Linsky, 1980).

B – As it is established that cool giants have strong convective subphotospheric zones, the chromospheric heating may be due to short-periodic acoustic waves generated by the convective motions in the lower photosphere and dispersing as shock waves (Schmitz and Ulmschneider, 1980). In the wake of this train of waves, a reversal of temperature would provoke the excitation of Fe II and Mg II. In low-gravity stars, the acoustic waves are heavily damped when crossing the photospheric radiative zone and this prevents the growth of the shock discontinuity. The point where the temperature increase takes place due to shock dissipation (otherwise the temperature minimum), is far from the location of the shock formation. Because of the differences of abundances and ionization potential of Ca and Mg or Fe, the Ca II should be located in lower layers of the chromosphere than Mg II and Fe II. By comparison with the solar case, it should correspond to chromospheric layers between 5000° K and 8000° K. The absence of Ca II emission could then be explained if we suppose that Ca II is located in the region where the shock is not yet fully developed and where the energy is not sufficient to produce an emission. The irregular behaviour exhibited by the Fe II lines, for which we obtained strong observational evidence, may possibly be explained by a turbulent convection that gives rise to trains of acoustic waves of variable wavelengths.

C – The turbulent convective agitation may give rise to giant convective cells (Schwartzschild's hypothesis) which reach the surface of the stars and provide enough energy to sporadically extract relatively cool matter from the photosphere. Due to low gravity some of this material could escape and destroy the lower chromosphere. This mechanism would be similar to the one studied by Kafatos et al. (1979) and would give a time scale for M supergiants from 10 days up to 6 years between each photospheric eruption.

D – Another mechanism proposed by analogy with the Sun could be the following one: the variable Fe II emission lines should be caused by a discrete magnetic structure in the chromosphere whenever the field lines—which originate in the magnetic tubes existing in the photosphere—converge (for example, Tinbergen and Zwaan, 1981). However, it is not known whether the C-type stars have sufficiently strong magnetic fields. These stars have convective zones, but due to their small rotational velocities ($V \times \sin i \leq 10 \text{ km s}^{-1}$) the classical dynamo principle must be excluded and the present hypothesis should only rely on a local dynamo mechanism similar for example to the one studied by Robinson and Durney (1982) for main-sequence stars.

The Circumstellar Shell

Fig. 3 shows the observed spectral energy distribution of TW Hor near maximum luminosity, together with predicted emer-

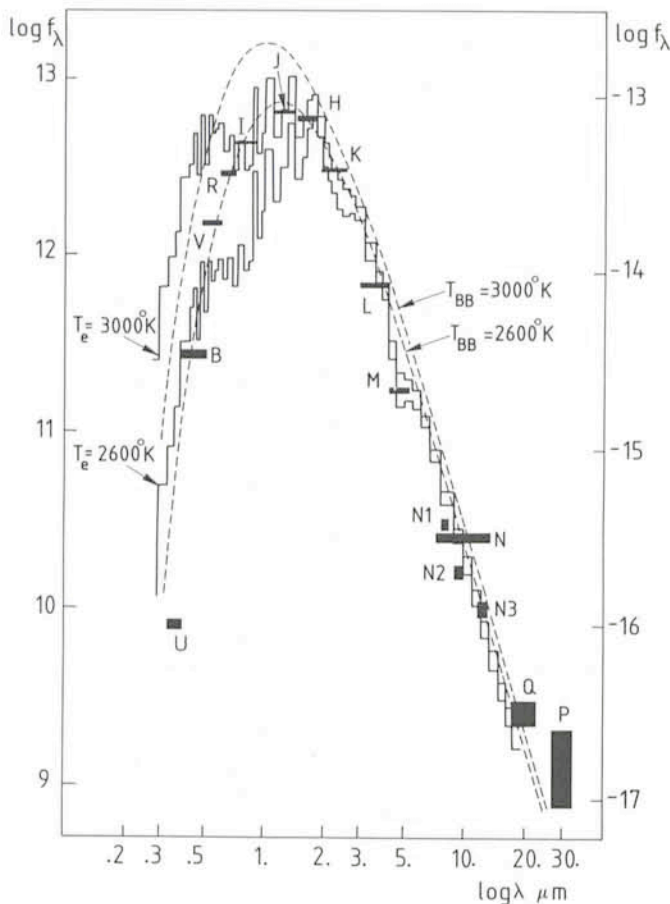


Fig. 3: Broad and narrow pass-band photometry of the star TW HOR, near maximum luminosity ($\varnothing = 0.89$). UBVRI photometry was carried out at the ESO 50 cm telescope with its standard photometer and Quantacon photomultiplier on September 14, 1981. JHKLM photometry was performed with the ESO standard InSb photometer attached to the 1 m telescope, during the same night. 10 μm to 30 μm photometry was performed on the following night with the standard ESO-bolometer attached to the 1 m telescope. Note that filters N, N1, N2 and N3 do not have BaF₂ blocking filters to suppress leaks longward of 20 μm .

The step-shaped solid lines are the predicted emergent line-blanketed fluxes from model atmospheres with $T_e=3000^\circ\text{K}$ and $T_e=2600^\circ\text{K}$. The continuous lines are the black-body curves for the same temperatures: $T_{BB}=3000^\circ\text{K}$ and $T_{BB}=2600^\circ\text{K}$. The right ordinate scale gives the logarithm of the observed fluxes in $\text{W}/\text{cm}^2/\mu\text{m}$. The left ordinate scale gives the logarithm of the predicted fluxes in $\text{erg}/\text{cm}^2/\text{sec}$ per $\Delta\lambda=1 \text{ cm}$.

gent fluxes of blanketed model atmospheres (Querci and Querci, 1976) with the effective temperatures $T_e=3000^\circ\text{K}$ and $T_e=2600^\circ\text{K}$. The other parameters of the model atmospheres are a gravity $g=1 \text{ cm}/\text{sec}^2$, a turbulent velocity $V=5 \text{ km}/\text{sec}$ and a chemical composition appropriate to the photosphere of carbon stars, named DE12 in the quoted reference. The molecular line blanketing taken into account in the models comes from the CO, CN and C₂ molecules, and the continuous opacity sources are the free-free, bound-free and scattering ones specific to cool stars.

From the V, R, I, J, H, K, L and M bands it can be seen that the effective temperature of the star is such as $2600^\circ\text{K} < T_e < 3000^\circ\text{K}$. Concerning the J, H, K, L bands, Tsuji (1981) reports that N-type irregulars — i. e. SRb type of variability applicable to TW Hor — are observed free from dust thermal emission. Also, this author demonstrates that the L flux is a good quasi-continuum, the HCN and C₂H₂ absorptions being situated at

the edge of the L-band at 3 μm . In the absence of detailed spectrophotometric observations on the near-IR region of TW Hor, we consider that this star follows these general outlines.

As for the M-band, the absorption is due to CO (photospheric and circumstellar) and possibly to C₃ at 5.2 μm .

Now, let's examine the spectral range of the U and B bands where for the carbon stars the theoretical fluxes are above the black body and the observed ones are fairly below. These apparent discrepancies may be partly due to a neglect of atomic and SiC₂ and C₃ molecular blanketing in our theoretical opacities, such that the predicted fluxes are too high. This is confirmed by the detection of the infrared crystalline SiC (see below) which is a solid condensate of gaseous SiC₂ and implies the presence of this last molecule in the UV region of TW Hor. Moreover, as quoted by Bergeat et al. (1976a), absorption by small SiC and graphite grains could, at $\lambda < 0.5 \mu\text{m}$, increase the discrepancy between observed and predicted fluxes, because the opacity of grains has not been included in the atmosphere models. TW Hor is among the carbon stars having a high near-UV luminosity with its colour indices $B - V = 2.5$ and $V - B = 3.3$, so observed V and B values are nearer the predicted fluxes than those of many other carbon stars.

In the far-infrared part of the curves, the excesses visible in the N, Q and P bands clearly prove the presence of a circumstellar shell in TW Hor. The small excess at 11.2 μm in the N-band with respect to N1, N2 and N3 is due to the SiC emission band. Note that spectrophotometric observations of TW Hor (Bouchet, 1983) show an intense emission by SiC, while the large N-band with its effective wavelength at 8.8 μm cannot justify it fully. The emission in the Q-band at 22.5 μm reminds the one first seen by Goebel et al. (1980) in the carbon star Y CVn. On the other hand, though our theoretical energy distribution curves stop around 20 μm , an emission is evident in the P-band and would be due to an unidentified circumstellar emission previously pointed out by Hagen et al. (1975) in some cool stars. We have to emphasize that possible free-free emission from chromospheric H and H⁻ would contribute to the observed infrared excess, besides the circumstellar shell.

That a circumstellar shell is present around TW Hor seems obvious from the above considerations. Further arguments may be added, such as the colour difference $[11 \mu\text{m}] - [3.5 \mu\text{m}] = -0.65$, well known photometric shell indicator. Nevertheless, this goes against the classification by Bergeat et al. (1978) who stipulate that TW Hor is a star without shell. In fact, these authors give this star an effective temperature $T_e = 2530^\circ\text{K}$. However, from Fig. 3 it appears that TW Hor has a temperature certainly superior to 2600°K and rather close to 3000°K (an accurate value is being computed through a run of model atmospheres). So, if we adopt, say, $T_e = 2800^\circ\text{K}$ and if we take into account the photometric data that we got: $(R+I) - (J+K) = 4.7$, these values locate TW Hor among the non-Mira stars with shell in the Fig. 1 of Bergeat et al. (1976b). Moreover, our adopted temperature together with our value $(R+I) - 2J = 3.3$ would not be out of range in the $(R+I) - 2J$ index versus T_e figure of these authors, which illustrates the effective temperature scale that they proposed.

Conclusions

The important result reported in this paper is that, for the first time, chromospheric variable activity has been detected in a cool low-gravity star of the carbon class. Though the mechanisms able to heat the chromosphere are not yet well understood, this would shed some light on the problems concerning chromospheres. For instance, the validity of the Wilson-Bappu relations for CaII and MgII (Linsky, 1980) should be carefully considered in this particular case. Let us recall that these

relations are simple correlations between CaII or MgII emission core widths and stellar absolute visual magnitude. High-resolution UV observations with IUE are planned for TW Hor which appears relatively bright in the ultraviolet range. High resolution on CaII H and K lines are undertaken at various phases with the La Silla Coudé Echelle Spectrometer (CES) to decide about re-emission in the line cores.

In short, we show that the outer layers of TW Hor consist in a photosphere ($T_e \sim 2800^\circ\text{K}$), a warm chromosphere ($5000^\circ\text{K} < T < 8000^\circ\text{K}$) and a circumstellar shell. This situation is not greatly dissimilar with what has already been seen in M giants of late type, but with different temperatures. It can be reasonably thought that this may be extended to other carbon stars. Its relative high UV luminosity enabled us to detect in TW Hor what may exist in UV-fainter stars as well. A conspicuous feature is the strong ultraviolet absorption underlined by the theoretical flux curves of carbon stars, contrary to the M stars (Tsuji, 1976): this is the best proof of the presence of dust grains absorbing in the UV spectral range of C stars.

Acknowledgements

It is a pleasure to thank Mr. D. Hofstadt and the technical staff of La Silla who are always very helpful. Special thanks go to Messrs. M. Bahamondes, L. Ramirez and H. Vega for night-assistance and initiatives when taking coudé spectra. The assistance of Mr. R. Vega for the infrared observations was also very valuable, as was the help of Mrs. B. Pech (Pic-du-Midi Observatory) in the improvement of the spectra reduction programmes.

One of us (P.B.) is grateful to Drs. A. Ardeberg, A.C. Danks and H. Pedersen for beneficial suggestions when preparing the draft of this paper and to Drs. P.S. The, J. Koornneef and D. Gillet for helpful discussions.

References

- Bergeat, J., Sibille, F., Lunel, M., Lefèvre, J., 1976 a, *Astron. Astrophys.* **52**, 227.
 Bergeat, J., Lunel, M., Sibille, F., Lefèvre, J., 1976 b, *Astron. Astrophys.* **52**, 263.
 Bergeat, J., Sibille, F., Lunel, M., 1978, *Astron. Astrophys.* **64**, 423.
 Bidelman, W.P., Pyper, D.M., 1963, *Publ. Astron. Soc. Pacific.* **75**, 389.
 Boesgaard, A.M., Boesgaard, H., 1976, *Astrophys. J.* **205**, 44.
 Bouchet, P., 1983, *The Messenger*, same issue.
 Goebel, J.H., Bregman, J.D., Goorvitch, D., Strecker, D.W., Puetter, R.C., Russel, R.W., Soifer, B.T., Willner, S.P., Forrest, W.J., Houck, J.R., McCarthy, J.F., 1980, *Astrophys. J.* **235**, 104.
 Hagen, W., Simon, T., Dyck, H.M., 1975, *Astrophys. J.* **201**, L81.
 Herzberg, G., 1948, *Astrophys. J.* **107**, 94.
 Hill, S.J., Willson, L.A., 1979, *Astrophys. J.* **229**, 1029.
 Johnson, H.R., O'Brien, G.T., 1982, preprint.
 Kafatos, M., Michalitsianos, A.G., 1979, *Astrophys. J.* **228**, L115.
 Linsky, J.L., 1980, *Ann. Rev. Astron. Astrophys.* **18**, 439.
 Querci, M., Querci, F., 1976, *Astron. Astrophys.* **49**, 443.
 Querci, F., Querci, M., Wing, R.F., Cassatella, A. and Heck, A., 1982, *Astron. Astrophys.* **111**, 120.
 Robinson, R.D., Durney, B.R., 1982, *Astron. Astrophys.* **108**, 322.
 Schmitz, F., Ulmschneider, P., 1980, *Astron. Astrophys.* **84**, 191.
 Tinbergen, J., Zwaan, C., 1981, *Astron. Astrophys.* **101**, 223.
 Tsuji, T., 1981, *J. Astrophys. Astr.* **2**, 95.
 1976, *Publ. Astron. Soc. Japan* **28**, 567.

136 Austria – Observed at ESO

H.J. Schober, Institute for Astronomy, Graz, Austria

As an Austrian, I am happy to inform the ESO *Messenger* readers about photoelectric observations of the asteroid 136 Austria carried out successfully at ESO in February 1981 and just being published in *Astronomy and Astrophysics*.

This asteroid—discovered in 1874 by J. Palisa at Pola—is just a small object of only 41 km diameter with classification MEU-type which means that no type assignment was made: but it is definitely a bright asteroid with high reflectivity and does not belong to the darker C-type group.

My observations were carried out using the 0.6 m Bochum telescope during ESO time in February 1981. The nice result is shown in Fig. 1, where the four observing nights are overlapped, based on the resulting spinning period of $P = 11^{\text{h}}.5 \pm 0^{\text{h}}.1$ ($= 0^{\text{d}}.479 \pm 0.004$). Due to the compatibility of $2P = 23^{\text{h}}$, near a full day (and due to the short summer nights), it was not possible to get the complete rotation cycle. But the period

should be established pretty well—the light-curve amplitude is at least $0^{\text{m}}.40$, and the mean V-magnitude of 136 Austria was about $V = 13.30$; the light-curve shows double-wave characteristic with nearly identical primary and secondary maxima; the secondary minimum was never observed.

The reader interested a little bit more in the general aspect of photoelectric observations of asteroids is advised to refer to earlier articles published in the ESO *Messenger* by H.J. Schober in No. 24 (1981) or by H.J. Schober and J. Surdej in No. 29 (1982).

I think I was especially lucky to have finally observed this asteroid at ESO—also in honour of my own country—and I would like to express my gratitude to Prof. L. Woltjer on behalf of ESO, for having allotted so much telescope time to me, though Austria is not a member state of ESO. I should also make my acknowledgements to the "Austrian Research Fund", projects 3136/4852, which helped to cover my travel expenses for those observations!

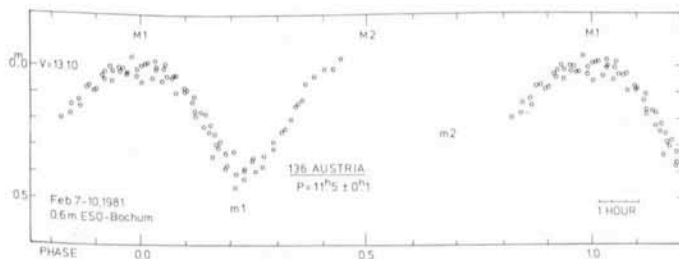


Fig. 1: Overlap of photoelectric observations for the asteroid 136 Austria, obtained in four nights, Feb. 7–10, 1981 with the 0.6 m Bochum telescope at La Silla. The rotation period of 136 Austria is $P = 11^{\text{h}}.5$, all measurements were reduced to Feb. 10, 1981.

Applications for Observing Time at La Silla

Period 32 (October 1, 1983 – April 1, 1984)

Please do not forget that your proposals should reach the Section Visiting Astronomers **before April 15, 1983.**

Visiting Astronomers

(April 1 – October 1, 1983)

Observing time has now been allocated for period 31 (April 1 – October 1, 1983). The demand for telescope time was again much greater than the time actually available.

The following list gives the names of the visiting astronomers, by telescope and in chronological order. The complete list, with dates, equipment and programme titles, is available from ESO-Garching.

3.6 m Telescope

- April: Engels/Perrier, Kunth, D'Odorico/Rosa, Perinotto/Purgathofer, Shaver/Robertson, Reipurth, Kudritzki/Méndez/Simon, Mouchet/Motch/Bonnet-B., Illovaisky/Chevalier/Motch/Bezanger, de Jong/Habing/Wesselius.
- May: de Jong/Habing/Wesselius, de Jong/Willems, Kollatschny/Fricke, Foy/Bonneau, Boisson/Péquignot/Ulrich, Crane/West/Valentijn/Kruszewski, Bertola/Galletta, Tarenghi, Cetty-Véron/Véron/Tarenghi, Fossat/Grec, Eichendorf, Moorwood/Glass.
- June: Moorwood/Glass, Moorwood, Papoular/Pégourie, Koester/Reimers, Koester/Weidemann, Schild/Maeder, Sherwood/Gemünd.
- July: Sherwood/Gemünd, Steppe/Witzel/Biermann, Schultz, Sieber/Wielebinski/Kreysa/Gemünd, Macchetto/Perryman/di Serego Alighieri/Capaccioli/Perala/Castellani/Caputo/Miley/Heckman, Gillespie/Krügel/Schulz/Lauter, Pedersen.
- August: Pedersen, Pedersen/Motch/Hurley/Pizzichini/Danziger/Tarenghi, Danziger/Pedersen, Shaver/Robertson, Moffat/Shara, Bergvall/Ekman, Zuiderwijk/de Rooter, Danziger/de Rooter/Kunth/Lub, Danziger/Maraschi/Tanzi/Treves, de Jong/Habing/Wesselius, Leitherer/Wolf/Stahl/Zickgraf, Véron.
- Sept.: Véron, Azzopardi/Breysacher/Lequeux/Maeder/Westerlund, Jörgensen/N.-Nielsen, Bergeron/Kunth, Barbieri/Nardon/Cristiani, Houziaux/Nandy, Ardeberg/Lindgren/Nissen.

1.4 m CAT

- April: Andersen/Rucinski/Staniucha, Spite, F. & M., Gillet/Maurice/Bouchet, Barbuy, Soderblom, Soderblom/Avrett, Gillet/Maurice/Bouchet.
- May: Gillet/Maurice/Bouchet, Roueff/Felenbok/Czarny, Frisk/Edvardsson/Gustafsson, Gratton/Ortolani, Gondoin/Mangeney/Praderie, Gillet/Maurice/Bouchet, Danks/Lambert.
- June: Danks/Lambert, Baade, Baade/Pollok, Baade/Danziger, Gillet/Maurice/Bouchet, Ferlet/Baade, Ferlet/Vidal-Madjar/Gry/Dennefeld, Tjin A Dje/Thé.
- July: Gillet/Maurice/Bouchet, Furenlid, Pallavicini/Pakull, Gillet/Maurice/Bouchet.
- August: Gillet/Maurice/Bouchet, Yorke/Schallwich, Lührs.
- Sept.: Butcher, Gerbaldi/Faraggiana/Floquet/van Santvoort.

1.5 m Spectrographic Telescope

- April: Chmielewski/Jousson, Spite, F. & M., Dumont/Maurice, Rosa, Joubert/Kunth, Dumont/Maurice, Perinotto/Purgathofer, Reipurth, Dumont/Maurice, Grewing/Krämer/Schulz-Lüpertz/Bianchi, Stenholm.
- May: Stenholm, Fricke/Kollatschny/Yorke/Biermann, Lundström, Quintana/Melnick, Tarenghi, Bettoni/Galletta,

de Loore/van Paradijs/Zuiderwijk, Gondoin/Mangeney/Praderie, Dennefeld/Stasinska.

- June: Dennefeld/Stasinska, Dennefeld/Pottasch, West/Barbon/Capaccioli, Alloin/Pelat, Thé/Westerlund, Houziaux/Heck/Manfroid, Tanzi/Pakull/Tarenghi.
- July: Tanzi/Pakull/Tarenghi, Richtler/Seggewiss, Sadler, Metz/Häfner, Schulte-Ladbeck, Hoffmann/Duerbeck.
- August: Hoffmann/Duerbeck, Bergvall/Ekman, Zickgraf/Stahl, Bertout/Bouvier, Danziger/Maraschi/Tanzi/Treves, Wargau/Drechsel/Rahe, Jensen.
- Sept.: Jensen, Véron, Pelat/Nottale, van Paradijs/Zuiderwijk.

1 m Photometric Telescope

- April: Engels, Wielebinski/Beck/Schnur/Loiseau, Bues/Rupprecht, de Jong/Willems, de Jong/Habing/Wesselius, Reipurth, Pitault/Gomez.
- May: Pitault/Gomez, Lundström, Liller/Alcaíno, Brand/Wouterloot, Barbieri/Romano/Cristiani, Oliva/Moorwood/Calamai, Eichendorf.
- June: Eichendorf, Vogt, Wendker/Heske, Koester/Weidemann, Westerlund/Thé, Houziaux/Heck/Manfroid, Tanzi/Pakull/Tarenghi.
- July: Tanzi/Pakull/Tarenghi, Houziaux/Heck/Manfroid, Sadler, Richtler, Gillespie/Krügel/Schulz/Lauter, Heck/Manfroid.
- August: Heck/Manfroid, Bertout/Bouvier, Bergvall/Ekman, Leitherer/Wolf/Stahl/Zickgraf, de Jong/Habing/Wesselius, Chini.
- Sept.: Chini, Cetty-Véron, Gammelgaard/Kristensen, Houziaux/Nandy, Epchtein/Braz.

50 cm ESO Photometric Telescope

- April: Wielebinski/Beck/Schnur/Loiseau, Scaltriti/Cellino/Zappala/Di Martino, Leandersson.
- May: Leandersson, Liller/Alcaíno, Frisk/Edvardsson/Gustafsson, Mauder.
- June: Mauder, Thé/Westerlund.
- July: Metz/Häfner, Moreno/Carrasco, Schulte/Ladbeck/Leitherer.
- August: Schulte/Ladbeck/Leitherer, Zickgraf/Stahl, Leitherer/Wolf/Stahl/Zickgraf, Sterken-group.
- Sept.: Sterken-group.

GPO 40 cm Astrograph

- April: De Sanctis/Zappala/Lagerkvist/Debehogne.
- May: Amieux.
- June: Giesecking/Dettmar.
- August: Debehogne/Machado/Caldeira/Netto/Vieira/Mourao/Tavares/Nunes/Bezerra/Zappala/De Sanctis/Lagerkvist/Protitch-B.

1.5 m Danish Telescope

- April: Mouchet/Motch/Bonnet-Bidaud, Illovaisky/Chevalier/Motch/Bezanger.
- May: Grewing/Krämer/Schulz-Lüpertz/Bianchi, Boisson/Pequignot, Loose/Fricke/Schallwich/Thuan, Danziger/Sol, Danziger/D'Odorico/Pedersen, Ortolani/Gratton, Pedersen, Vigroux/Souviron/Kunth, Bergeron/Kunth.

June: Andersen/Nordström/Olsen, Lindgren, Ardeberg.
 July: Ardeberg, Ardeberg/Lindgren, Mayor/Burki, Mayor/Mermilliod, Ilovaisky/Chevalier/Motch/Hurley, Ilovaisky/Chevalier/Motch/Bezanger.
 August: Prévot/Imbert/Maurice/Andersen/Nordström/Benz/Mayor/Ardeberg, Maurice, Pedersen.
 Sept.: Pedersen, Fusi Pecci/Battistini/Bonoli/Buonanno/Corsi, Pedersen/Pizzichini, Cetty-Véron/Véron/Tarenghi/Petersen, Testor/Lortet/Heydari-Malayeri.

50 cm Danish Telescope

May: Grenon/Hög.
 June: Grenon/Hög, Vander Linden.
 July: Vander Linden.

90 cm Dutch Telescope

April: de Zeeuw/Lub/de Geus/Blaauw.
 May: de Zeeuw/Lub/de Geus/Blaauw, Brand/Wouterloot.
 June: Tanzi/Pakull/Tarengi.
 July: Tanzi/Pakull/Tarengi, Barwig/Ritter, Bruch.
 August: Diethelm.
 Sept.: Diethelm, v. Paradijs/v. Amerongen.

61 cm Bochum Telescope

April: Sterken-group.
 May: Sterken-group, Terzan, Vogt.
 June: Vogt, Wendker/Heske, Metz/Häfner.
 July: Metz/Häfner.

Mechanics and the Stars

S. Balon, ESO

The ESO engineering workshop has recently acquired a universal "Tool Room Milling and Boring Machine" with computer control or, in more technical terms, "Continuous Path Control" (Fig. 1).

The production of parts with complicated contours is now possible with programmes which can be entered directly by the operator from a terminal in the lab (Fig. 2). In this way the technician has on the display screen a continuous check of the programme throughout its execution: He can see at any given time the next instruction to be carried out and he can also check the characteristics of the tool in use, e.g. length, radius and spindle speed, direction for the tool radius compensation.



Fig. 1: S. Balon working with the new "Milling Machine" in the ESO workshop.

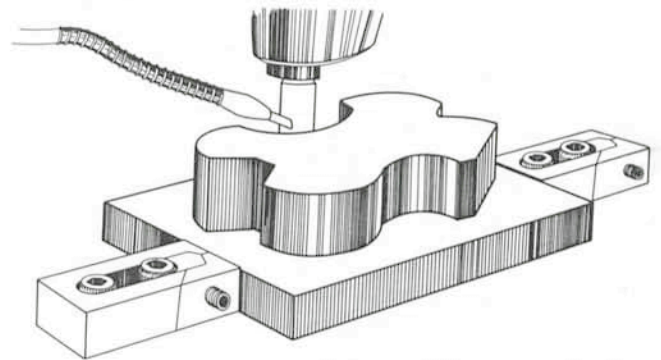


Fig. 2: This is a schematic illustration of a complicated piece being milled on the machine table.

The concept of the machine with recirculating ball screws in three axes completely eliminates backlash, thus permitting to achieve linear interpolation, inclined straight lines, circular interpolation, rounding of corners from straight lines to arcs, tangential approach of a contour at a defined point on a circle, absolute and incremental position set values, and entry of position – metric or imperial as selected. It is now possible to achieve radii up to 20 metres with an accuracy of five microns, which previously was very difficult to do with conventional machines.

The entries can be made in rectangular coordinates or in polar coordinates.

There are also some fixed programme cycles such as peck drilling, thread tapping, groove, pocket (rectangular and circular) milling, 3D straight lines, displacement of the zero point (useful for repetition with the help of sub-programmes of different contours at desired intervals), mirror images (x, y and z axis).

It is of course possible to use this machine in manual control mode via the electronic handwheel.

This handwheel with ten ranges of sensibility is switchable to each of the three axes, given for one revolution a displacement of the tables ranging from 10 mm to 0.02 mm according to the choice of the sub-division factor.

We can also appreciate the hydraulic quick action system for tool retention on horizontal and vertical spindle.

It would take too much time to describe all of this powerful new machine. But we can already appreciate the accuracy for example in the realization of the holes for the support of the fiber optics in the masks for this promising highly advanced instrument, already tested by Daniel Enard and Massimo Tarengi at the 3.6 m telescope in November 1982. I am referring to the "Multiple Object Spectrograph".

Star Formation and Interstellar Matter in the Large Magellanic Cloud

J. Isserstedt, Institut für Astronomie und Astrophysik der Universität Würzburg

A glance on the very recent history of star formation in a galaxy seems to become possible by investigating the distribution of stars as function of their ages and comparing it with the distribution of interstellar matter. In our Galaxy such investigations are extremely difficult since distance determinations for stars and interstellar matter are not sufficiently accurate. This is due to the fact that neither the absolute magnitudes and intrinsic colours of luminous stars nor the reddening law of interstellar dust nor the kinematics of the neutral atomic interstellar hydrogen are precisely known.

The situation is far more favourable in the nearest extragalactic system, the Large Magellanic Cloud (LMC), which is very rich in young stars and interstellar matter. Kinematic investigations have shown that the luminous stars are concentrated to a rather flat rotating disk, which is seen nearly pole-on. Therefore the differences between the individual distances of the stars are small compared to their distances from the sun; in other words, all stars have nearly the same distance.

The Observations

Photoelectric photometry is needed for the age determination of the supergiants as well as for the determination of

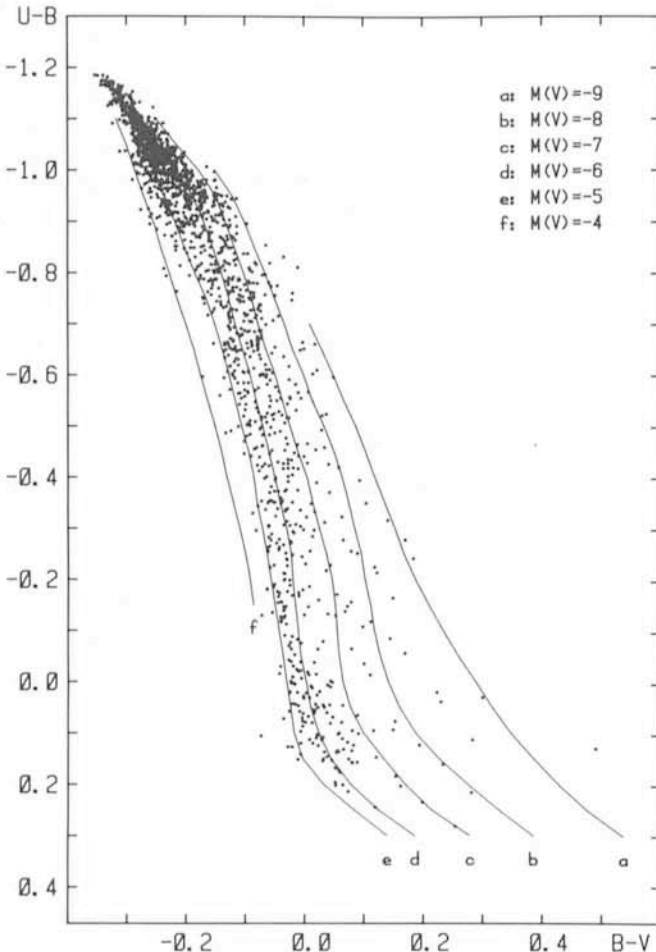


Fig. 1: The two-colour diagram of luminous stars in the LMC after correction for interstellar reddening.

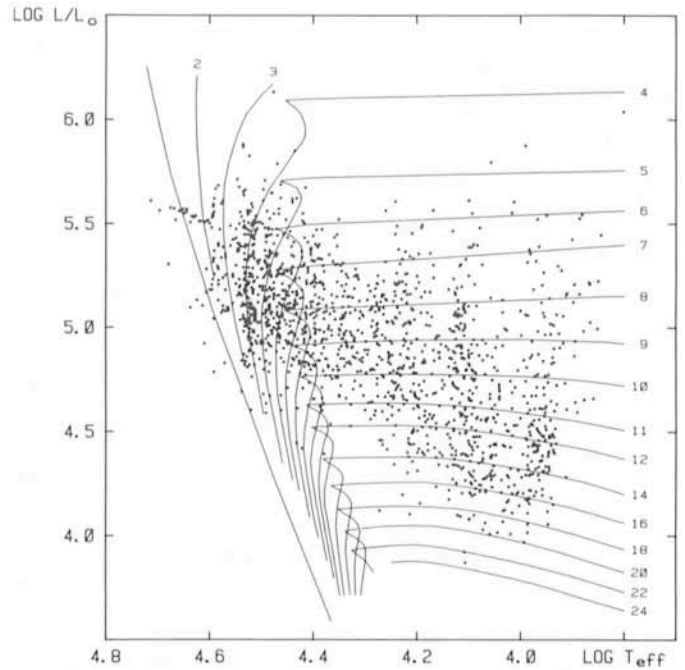


Fig. 2: The theoretical Hertzsprung-Russell diagram. The lines are isochrones. The ages are given in million years.

interstellar reddenings which are a measure of the amount of interstellar dust. Measurements in the UBV system are available now for approximately 1,600 members of the LMC. About 65% of these have been obtained by the author during three

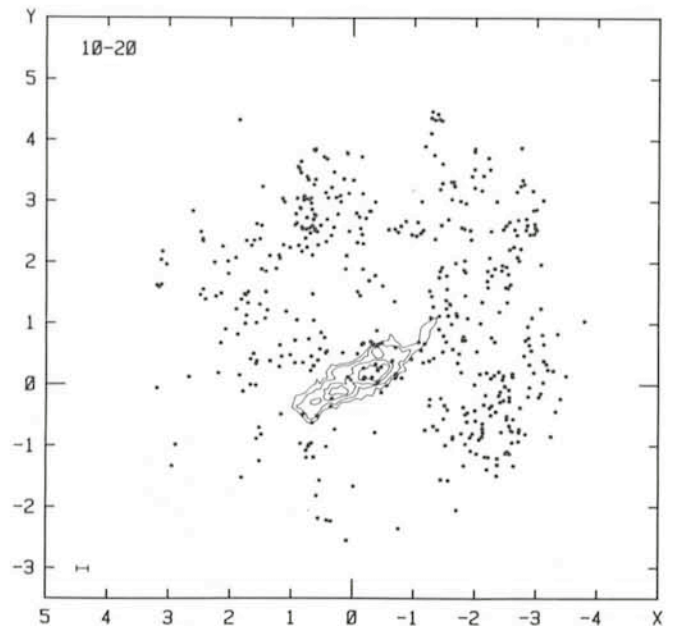


Fig. 3: The distribution of supergiants (filled circles) and Cepheids (squares) with ages between 10 and 20 million years. The coordinates are standard coordinates, their origin is in the optical centre of the bar. The isophotes (blue light) of the bar were taken from de Vaucouleurs (1957, *Astronomical Journal* **62**, 69). Due to their velocity dispersion of 10 km/s the stars have moved away from their places of formation by an average amount which is indicated in the lower left of the diagram.

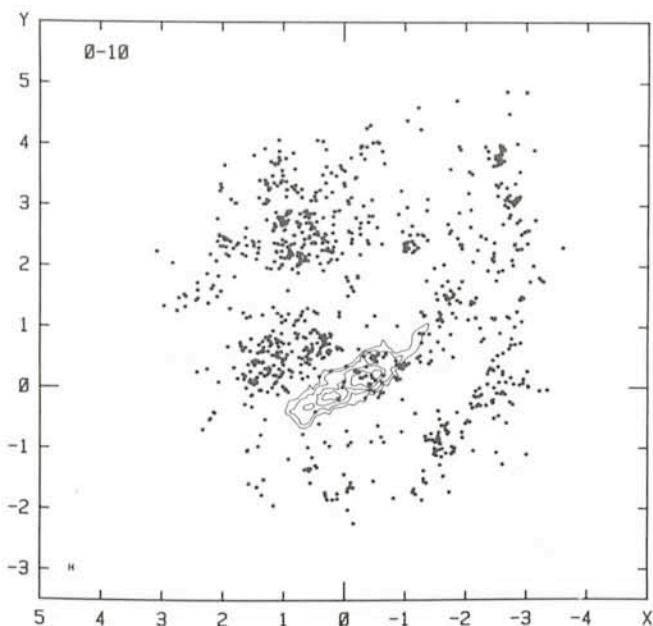


Fig. 4: The distribution of stars with ages up to 10 million years. For further explanation see Fig. 3.

observing runs at La Silla with the 61 cm telescope. The remaining part has been measured by various other groups mainly with the 1 m telescope and partly again with the 61 cm telescope. To carry out photometry for so many stars needs a lot of observing time, which is not available with the over-requested large telescopes. This emphasizes the importance of the smaller instruments for long lasting observing programmes.

The Determination of Interstellar Reddenings and Ages

The interstellar reddenings were derived from the positions of the stars in the two-colour diagram. For this purpose one has to know the intrinsic relations $(U-B)_0$ vs. $(B-V)_0$ for unreddened

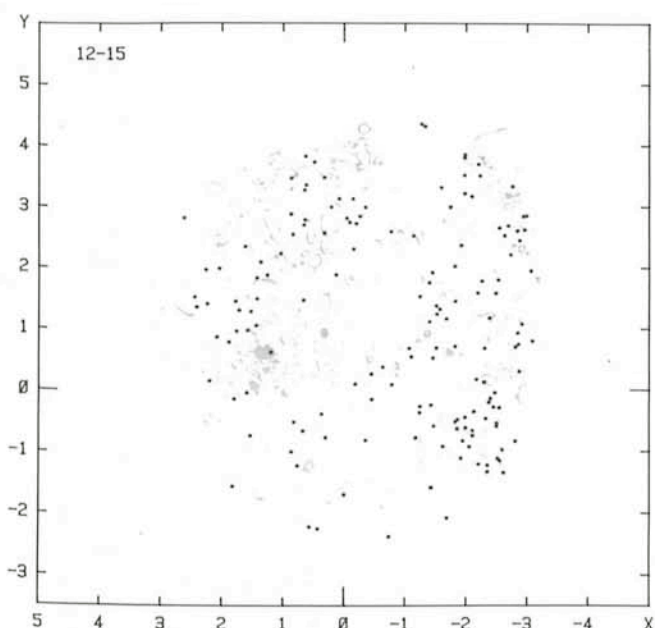


Fig. 5: The distribution of supergiants (filled circles) and Cepheids (squares) with ages between 12 and 15 million years. Also shown are the HII regions.

stars. It has been shown by several authors that these relations depend on the absolute magnitude of the stars and that they are in the Magellanic Clouds different from those in our Galaxy. A reliable age determination requires a very precise calibration of these intrinsic relations especially for those stars which are still rather near to the upper main sequence in the Hertzsprung-Russell diagram. To allow the present investigation it was therefore necessary to redetermine the intrinsic colours (Isserstedt, 1982, *Astronomy and Astrophysics* **115**, 97). Fig. 1 shows the two-colour diagram for the luminous stars in the LMC after correction for interstellar reddening together with the magnitude-dependent relations for unreddened stars. One realizes that most of the stars are early-type stars and that the data become very incomplete below absolute magnitudes $M_V = -5^m$.

The ages of the stars have been derived by comparison with evolutionary calculations (Maeder, 1981, *Astronomy and Astrophysics* **99**, 97; **102**, 401 case B with moderate mass loss). Fig. 2 shows the stars in the theoretical Hertzsprung-Russell diagram after transformation of the intrinsic colours and absolute magnitudes into temperatures and bolometric luminosities, respectively. Also shown are the isochrones which were interpolated from the evolutionary tracks.

The Distribution of Supergiants

The data on supergiants were combined with data on Cepheids available in the literature and used for the production of a little computer film displaying the distribution of stars as function of age. Two frames of the film are shown in Figs. 3 and 4. (The whole time series and a detailed discussion will appear in *Astronomy and Astrophysics* soon). Note the rapid structural change between these two age groups and especially the formation of the two huge associations 30 Doradus ($X = 1^{\circ}.2$; $Y = 0^{\circ}.7$) and Shapley III ($X = 0^{\circ}.6$; $Y = 2^{\circ}.4$). Figs. 5-8 present the distributions of supergiants and Cepheids for smaller age intervals together with the regions of ionized hydrogen (taken from Davies et al., 1976, *Memoirs of the Royal Astronomical Society* **81**, 89). Note again the formation and time-dependent growth of Shapley III and the burst of star formation around 30 Doradus.

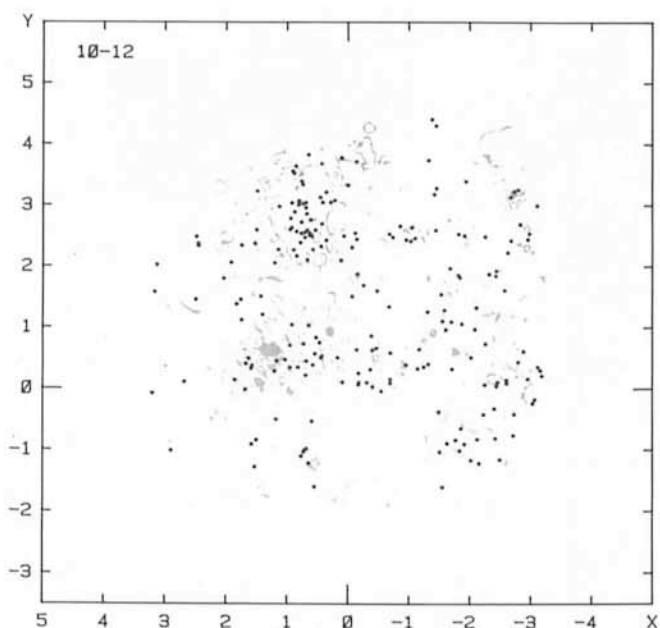


Fig. 6: The distribution of supergiants and Cepheids with ages between 10 and 12 million years.

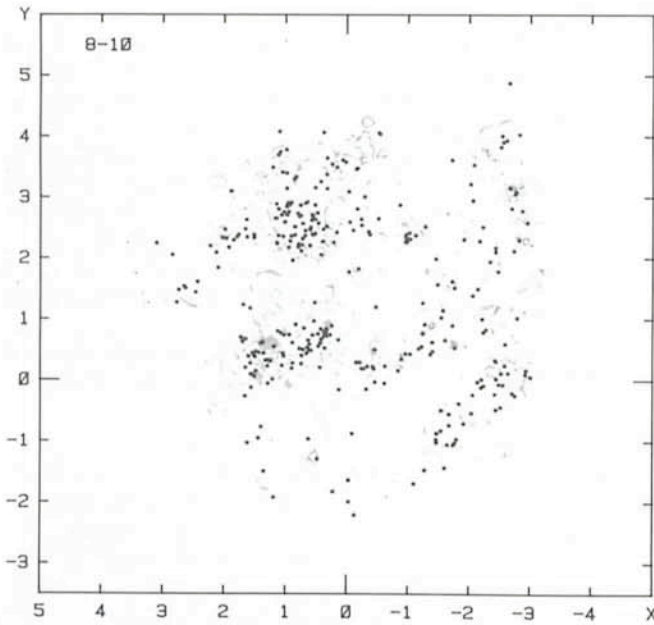


Fig. 7: The distribution of supergiants and Cepheids with ages between 8 and 10 million years.

The Distribution of Interstellar Matter

In a forthcoming paper (Isserstedt and Kohl, in preparation) it will be shown that the star formation rate *in the past* $T \approx 10^7$ years) is on average over the LMC proportional to the *nowadays* observed column density of neutral interstellar hydrogen HI, but that there is no correlation whatsoever between this star formation rate and the density of interstellar dust. This leads to the hypothesis that the dust is partly embedded in clouds of molecular hydrogen H_2 which seem to occur more often in regions where the star formation rate in the past was rather low (and might perhaps be high in the future).

The isodensities in Fig. 9 are describing the distribution of interstellar dust in the LMC. Reddening from dust in the galactic foreground has been subtracted. The sequence "white-grey-

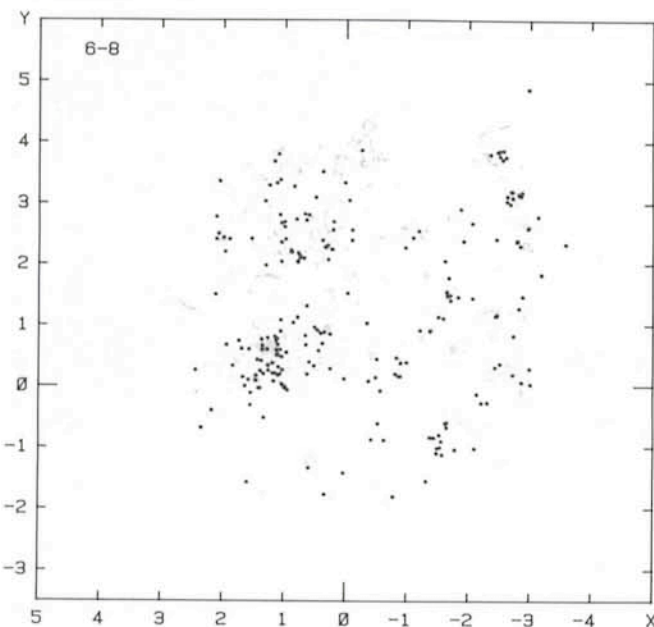


Fig. 8: The distribution of supergiants and Cepheids with ages between 6 and 8 million years.

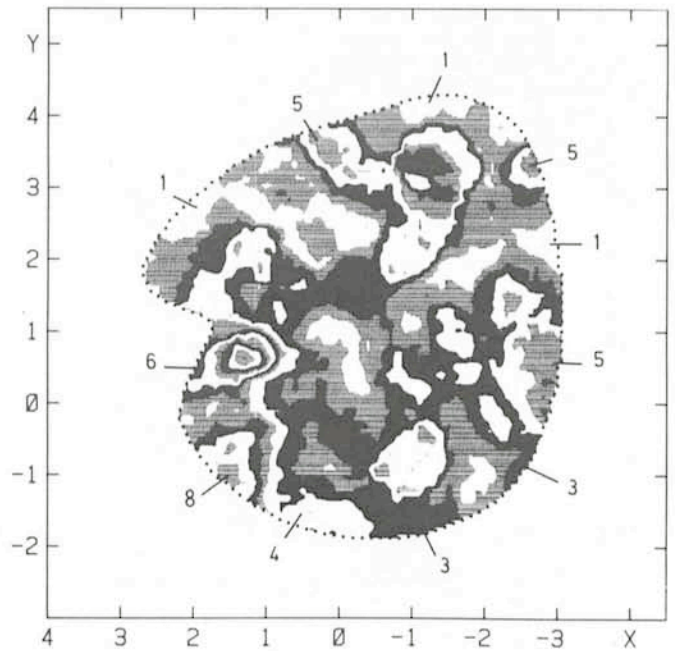


Fig. 9: Isodensities of interstellar reddening after subtraction of reddening from the galactic foreground. One step corresponds to $\Delta E = 0''.02$.

black-white ..." denotes increasing reddening. One step corresponds to $\Delta E = 0''.02$. Note that the Shapley III association has a low dust content but is surrounded by an extended cloud complex, while the otherwise similar association 30 Doradus contains far more interstellar dust. It is interesting to compare Fig. 9 with the distribution of atomic hydrogen from 21 cm measurements (McGee and Milton, 1964, *IAU Symposium 20*, 291). In spite of some common features in both distributions they are mostly quite dissimilar. This again might be explained if the dust is partly embedded into extended regions of molecular hydrogen, which are otherwise not so easily observable. If these results could be confirmed by independent methods this might have severe consequences for our understanding of star formation and the development of large scale structures in galaxies.

List of Preprints Published at ESO Scientific Group December 1982 – January 1983

221. I.J. Danziger: Optical Properties of Supernova Remnants. To appear in the proceedings of the IAU Symposium 101 "Supernova Remnants and Their X-ray Emission", Venice, Sept. 1982. December 1982.
222. J. Koornneef: Near-Infrared Photometry. Paper I: Homogenization of Near-Infrared Data from Southern Bright Stars. *Astronomy and Astrophysics Suppl.* December 1982.
223. S. D'Odorico and M. Dopita: Chemical Abundances in the Interstellar Medium of Galaxies from Spectrophotometry of Supernova Remnants. To appear in the proceedings of the IAU Symposium 101 "Supernova Remnants and Their X-ray Emission", Venice, Sept. 1982. December 1982.
224. I. Semeniuk: Core Radii Determination for 11 Southern Clusters of Galaxies. *Acta Astronomica.* December 1982.
225. C.-I. Björnsson: A New Look at Pulsar Polarization. *Astrophysical Journal.* December 1982.
226. G.L. Chincarini, R. Giovanelli and M.P. Haynes: On the Geometry of Two Superclusters Coma-A 1367 and Perseus-Pisces. *Astronomy and Astrophysics.* December 1982.

227. G.L. Chincarini, R. Giovanelli and M. P. Haynes: 21 cm Observations of Supercluster Galaxies: The Bridge Between Coma and A 1367. *Astrophysical Journal*. December 1982.
228. R. Braun, W. M. Goss, I.J. Danziger and A. Boksenberg: The Kinematics of the SNR G 292.0+1.8. To appear in the proceedings of the IAU Symposium 101 "Supernova Remnants and Their X-ray Emission", Venice, Sept. 1982. December 1982.
229. E.J. Wampler: Observations of the MG II λ 2800 Spectral Region in Broad Absorption Line Quasars. *Astronomy and Astrophysics*. December 1982.
230. G.L. Chincarini, R. Giovanelli, M. Haynes and P. Fontanelli: Neutral Hydrogen in X-ray Cluster Galaxies: A 1367. *Astrophysical Journal*. December 1982.
231. G. Setti and G. Zamorani: Can All Quasars be Gravitationally Lensed Seyfert's Nuclei? *Astronomy and Astrophysics Letters*. December 1982.
232. W. Bijleveld and E. A. Valentijn: The Trivariate (Radio, Optical, X-ray) Luminosity Function of cD Galaxies I: New Westerbork Observations of 22 cD Galaxies and Einstein Observations of A 1918 and A 2317. *Astronomy and Astrophysics*. January 1983.
233. E.J. Wampler, C.M. Gaskell, W.L. Burke and J.A. Baldwin: Spectrophotometry of Two Complete Samples of Flat Radio Spectrum Quasars. *Astrophysical Journal*. January 1983.
234. A.C. Danks and D.L. Lambert: Interstellar C₂ in the Ophiuchus Clouds. *Astronomy and Astrophysics*. January 1983.
235. M.H. Ulrich and C. Boisson: The Ultraviolet Spectrum of the Seyfert Galaxies NGC 3516 and NGC 5548. *Astrophysical Journal*. January 1983.
236. P.A. Shaver and J.G. Robertson: Common Absorption Systems in the Spectra of the QSO Pair Q0307-195A, B. *Astrophysical Journal Letters*. January 1983.

The Telescope of Geneva Observatory and the Development of Geneva Photometry at La Silla

F. Rufener, Geneva Observatory

When Geneva Observatory set up its observing station at La Silla (Chile), the main objective was to extend its 7-colour photometric system to the southern hemisphere. Indeed, several programmes necessitated the covering of the whole celestial sphere.

Since November 1975, when the 40 cm telescope was put into operation and equipped with a photoelectric photometer for the Geneva 7-colour photometry, the Geneva station has experienced a series of development stages (cf. *Messenger* 6, 1976). This first photometer, simple and strong, was conceived for one optical channel with direct current detection registered by strip chart millivoltmeter. Various precautions were taken in order to stabilize the definition of the pass-bands, in particular by means of careful regulation of the temperature for the photomultiplier as well as for the filters and the main components of the measuring circuit. A differential photometer controlled by a minicomputer HP 2100 is in operation since 1977. This instrument works with a photomultiplier and a performant photon counting system (resolution time 50 ns). Behind a selective set of diaphragms, a quick sampling allows comparison of the flux arriving from both fields, one (A) on the optical axis and the other (B) taken on a chosen polar radius. This second field can be selected by the observer by varying the angular separation (ρ) of A and B and by choosing the direction (θ) of B relative to A by rotation of the photometer on its own axis.

The sampling of channels A and B takes place behind each of the seven filters of Geneva photometry, arranged on a wheel. Thus, at each revolution of this wheel, we have at our disposal 14 samples summed up on 14 counters. Most of the time beam A takes measures of a star while beam B measures the nearby sky. When the wheel is turning at a speed of 5 revolutions per second each sample is equivalent to an exposure time of about 14 milliseconds. Fourteen averages for each colour on each channel are recorded on magnetic tapes after approximately one minute of total exposure time. This time span allows the collection of 256 samples for each colour. Each mean value is recorded with statistical criteria established in real time. They are based on observed variances as well as on the theoretical variance of the signals. All this information indicates that registration of the measurements proceeds normally; it also allows a subsequent control of the measurement conditions. This photometer has been briefly described

by Burnet and Rufener (1979). The nature of the statistical criteria applied, their characteristics and their usefulness have been presented by Burnet (1976). A more detailed analysis by Bartholdi and Rufener will follow shortly. Mr. Burnet, an astronomy engineer who is stationed in Chile since 1977, has brought about several improvements to the controls of the



Fig. 1: The 70 cm telescope installed at La Silla in 1980. We notice on the optical axis the differential photometer which allows rapid sampling and on one of the Nasmyth focuses the photometer for occultations.

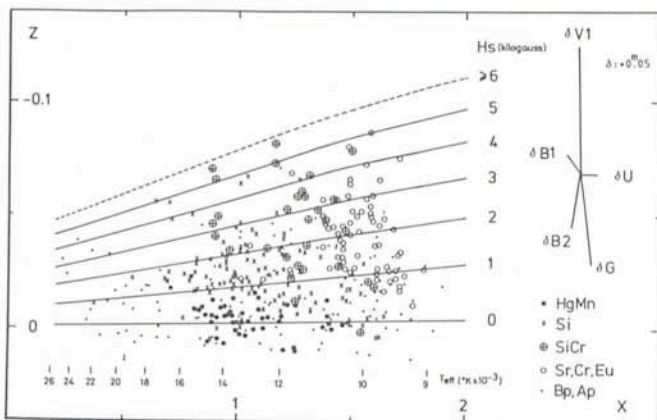


Fig. 2: On this plan of the photometric parameters X and Z one can identify several star categories showing spectral peculiarities recognized spectroscopically. The set of curves indicates the correlation of the parameter Z with the magnetic field H_s (Cramer and Maeder, 1980).

telescope and the dome. Both can now be positioned automatically on the basis of coordinates previously prepared by the operator. Two micro-processors determine and control the necessary displacements. Photometric measurements are recorded with all information on coordinates displayed by the telescope console during observation as well as the detailed state of the photometer. Over the years the steering programme of the photometer has been improved continually in order to obtain more complete information on the observations performed. This constant evolution has considerably improved the output and reliability of the observations.

In 1980 the 40 cm telescope was replaced by a 70 cm optical telescope on the equatorial table. Thus, an increase of 1.2 magnitude on the limiting magnitude could be obtained. The new telescope tube allows the Cassegrain focus on two Nasmyth positions to be moved. One of these focuses is equipped with a photometer specialized in recording star occultations by the moon. The diffraction fringes are registered simultaneously by two detectors. The signal transmitted by a dichroic beamsplitter is fed onto a photomultiplier with a pass-band centered on 450 nm. The reflected beam is fed onto a refrigerated diode with a pass-band centered on 900 nm. This equipment developed by P. Bartholdi can be put into operation very quickly. An interesting occultation can be registered in only 15 minutes. The controls of the telescope make it possible to observe not only the star eclipse behind the first quarter of the moon but also its appearance after the passage of the third quarter. These optical phenomena with a total time-span of several hundred milliseconds are registered in two colours, simultaneously with a 10 kHz frequency and time signals. Several unknown double stars have been discovered and some contributions to stellar diameter measurements have also been made possible.

However, the principal activity of this station remains photometric observation in the Geneva observing system. In 1980 the third edition of the Geneva photometric catalogue was compiled and published (Rufener, 1981). Over 14,600 entries reflect the main interests of the Swiss photometrists. The observers take turns in order to cooperate in a general programme resulting from the blending of individual research programmes. The observations and their reduction are dealt with in a single system centralized in Geneva. This contributes to maintaining intercomparison and homogeneity as systematic as possible. Two distinct procedures of processing and

weighing are carried out for the reduction of the "colours" (colour index relevant to colour B) and for obtaining the V magnitude whose pass-band is equivalent to the UBV system of Johnson-Morgan. The following is a brief description of programmes already started. Some of them are near completion, others are followed up closely and much effort is put into them. In the beginning, particular interest was taken in the study of the left part of the H-R diagram only, whereas today our effort is oriented towards the entire diagram.

– The observation of bright stars (Catalogue of Bright Stars) allows compilation of a large number of calibrations and comparisons with spectroscopic information as well as with other photometric systems. Many gaps in the knowledge about these stars have been filled.

– For B and A stars, three linear colour combinations determine three optimized and calibrated parameters. X for the effective temperature, Y for the absolute luminosity and Z for the estimation of the spectral peculiarity of these stars. Z represents a quantitative evaluation of the peculiarity. This evaluation is affected by the depression of the continuum at 5300 Å. Z is in close correlation to the existence of a strong magnetic field. Important samples of B and A stars are measured which have been selected from the catalogue by N. Houck; priority is given to all stars represented in the TD1 catalogue. These measurements are expected to yield an improved description of the galactic distribution of these stars

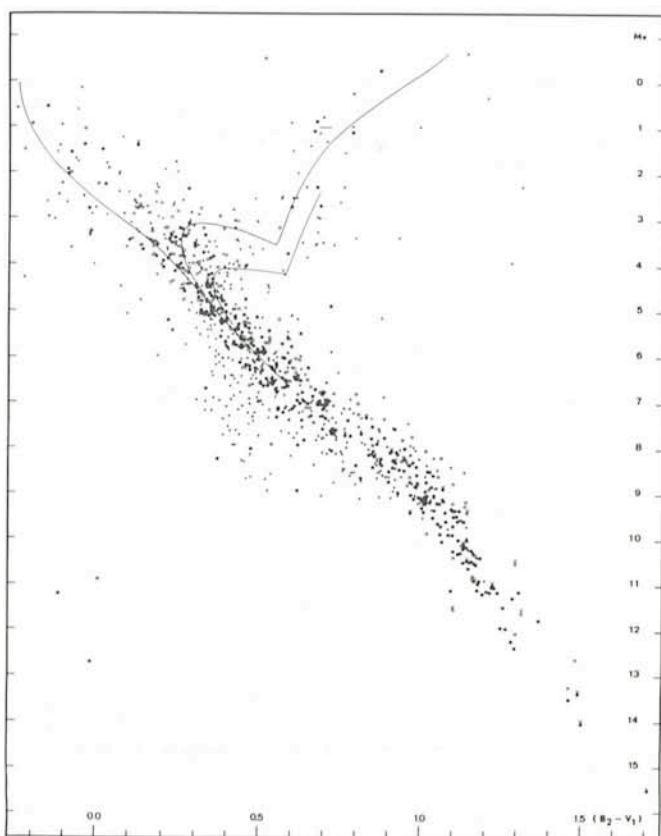


Fig. 3: Hertzsprung-Russell diagram obtained for 1077 stars in the Gliese catalogue. The photometric data of the Geneva catalogue have been associated with revised trigonometric parallaxes. Symbol explanation: \circ, \bullet : Stars with a probable error $\Delta M_v \leq 0.30$ mag.; $\times, +$: $\Delta M_v > 0.30$; \circ, \times : multiple stars. Complementary sign V shows the variability. Solid lines: sequences of the galactic clusters Pleiades and M67, and the probable limiting isochrone of the old disk population (Grenon and Rufener, 1981).

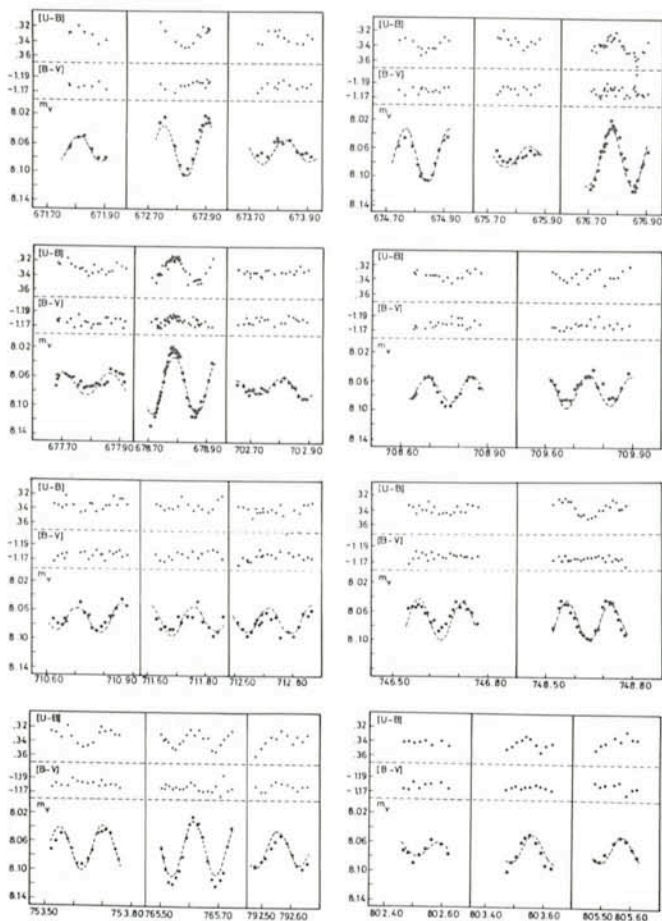


Fig. 4: Parts of the light curve of HD 129929, a star found to belong to β Cep category (2,444,000 days have been deducted from the Julian period). The harmonic analysis has yielded the three following periods and amplitudes:

PERIOD (days)	AMPLITUDE (Vmag.)
$P_1 = 0.154776$	0.0176
$P_2 = 0.143268$	0.0119
$P_3 = 0.155062$	0.0101

The presence of non-linear phenomena appears through the increase of the amplitudes observed during maxima and their decrease during minima (Waelkens and Rufener, 1983).

and of the interstellar matter together with a large list of unknown peculiar stars.

– Systematic measuring of O stars should contribute to a better description of the galactic structure on a large scale and to interstellar extinction laws.

– The instabilities observed in supergiant stars of all types, in β CMa type stars and in certain Ap stars are the subject of extensive observations in order to accumulate facts about the nature and recurrence of these phenomena. Several unusual stars have been discovered in this way. Some of them show three clearly distinguishable frequencies.

– A large number of galactic clusters have been observed with great care in order to get experimental sequences in the H-R diagram with a view to confrontations with theoretical models on star evolution.

– Studies of the fine structure components of the H-R diagram in the $T_{\text{eff}} \leq 6500^\circ \text{K}$ region are elaborated with stars

from the Gliese catalogue, cold stars in the Hyades and Praesepe, binary systems with important proper motions as well as stars in globular clusters. Applied to cold stars, Geneva photometry is an original means of determining some effects of temperature, luminosity, various chemical compositions, interstellar reddening or the simulating effects of binarity. These abilities have guided several programmes, such as:

– Analysis of the local population by means of critical tests on the membership and the search for cold stars belonging to spheres 10, 20 and 25 pc centered around the sun. Any suspected bias should be eliminated. The selection of new candidates is guided by kinematical criteria, spectral types and photometric classification.

– The study of old halo stars on the basis of local measurements of intermediate and population II stars within a sphere 50 to 100 pc; also by deep probing into regions close to the galactic poles. For this study the photometry of a large number of cold stars and often measurements of radial velocities are necessary.

– The development of an extensive programme covering all stars with large proper motion and a $m_v \leq 11.50$ detected in the Luyten's survey (NLTT). This project of long duration is on schedule for future observations with the satellite Hipparcos, the spectrovelocimeter CORAVEL and naturally with Geneva photometry.

– The concept of "photometric boxes", developed by M. Golay, makes it possible to select stellar samples with complete photometric similarity. The examination of possible divergences of their spectroscopic properties is always a source for improvement and refinement of stellar classification. The assumption of identical absolute magnitudes inside a photometric box has proven to be, for several fields of the H-R diagram, an original means for evaluating photometric parallaxes when a star with a known parallax is a member of the considered box. In application of this procedure, distances have been evaluated for 43 galactic clusters.

At the present time, the various programmes of Geneva photometry comprise a total of 31,500 stars. In the two hemispheres combined, close to 20,000 stars already have one or several measurements. Of the roughly 115,000 measurements in 7 colours gathered during the 23 years of Geneva photometric elaboration, more than two thirds will have been registered at La Silla.

I do not want to close this presentation without taking the opportunity to express my best thanks for the kind welcome at La Silla and to thank everyone who made a contribution to facilitate progress of this programme by his continuous help.

References

- Burnet, M. (1976) Thesis 235, Ecole polytechnique fédérale de Lausanne. Etude et réalisation d'un photomètre différentiel commandé par ordinateur.
- Burnet, M., and Rufener, F. (1979) *Astronomy and Astrophysics* **74**, 54.
- Cramer, N., and Maeder, A. (1980) *Astronomy and Astrophysics* **88**, 135.
- Golay, M. (1980) *Vistas in Astronomy*, **24**, 141.
- Grenon, M., and Rufener, F. (1981) *Astronomy and Astrophysics Suppl.* **46**, 25.
- Nicolet, B. (1981) *Astronomy and Astrophysics* **104**, 185.
- Rufener, F. (1976) *The Messenger*, **6**.
- Rufener, F. (1981) *Astronomy and Astrophysics Suppl.* **45**, 207.
- Waelkens, C.; Rufener, F. (1983) *Astronomy and Astrophysics*, in press.

Morphological and Physical Study of Planetary Nebulae

C. T. Hua, *Laboratoire d'Astronomie Spatiale de Marseille*, and R. Louise, *Faculté des Sciences d'Amiens and Observatoire de Marseille*

Summary

The photographic and spectrophotometric observations in order to carry out the "Monochromatic Atlas of Planetary Nebulae" are described. These observations are made in both hemispheres by using classical plates as well as modern receivers (IDS, Multiphot and Photon-Counting System). Preliminary results are presented.

Introduction

For years, Planetary Nebulae (PN) were thought to be expanding shells the interior of which is more or less filled with gas. A glance on direct photographs of familiar planetaries such as the Ring Nebula (NGC 6720), Helix (NGC 7293), Dumb-Bell (NGC 6853) or the Eskimo Nebula (NGC 2392) must convince us how complex their structure is. Although an ever increasing number of theories have been proposed since the Strömgren pioneering work (1939 *Astrophysical Journal* **89**, 526) some structure of PN remains unexplained (Louise, 1982, *Astronomy and Astrophysics Suppl.* **47**, 575). From the morphological point of view, a geometrical model must be built for each nebula. However, most people working on PN think or/and hope that they may be derived from a few geometrical models (2 or 3). Their difference from each other must be interpreted in terms of the evolution of a common main structure. Any evolutionary model needs an accurate knowledge of the physical parameters (T_e , N_e , relative abundances, etc.) and must take into account the interaction between an active nucleus with its surrounding interstellar matter (Louise, 1982, *Astronomy and Astrophysics* **102**, 303). This is important not only for studying planetary nebulae but also for understanding the general stellar evolution.

Observing Programme

Some features of PN structure can be interpreted directly from observations, others not or not yet because they require further investigations. If we examined in detail the large bibliography published within the last three decades concerning observational data of PN we could merely make the following comments:

(a) Direct photographs, monochromatic or not, are generally poor, inhomogeneous and photometrically underexploited. In some cases they are not suitable at all.

(b) Extensive spectrophotometric observations are generally performed for one or two points of a given nebula, rarely more. Only very few of the brightest PN have been accurately observed from point to point with a classical procedure. Today modern fast cameras such as IDS, CCD and photon-counting systems make available such observations for most PN, including the fainter ones.

(c) Since Minkowski's work (1964, *Publications of the Astronomical Society of the Pacific*, **76**, 197) faint nebulosities associated with PN are detected in some of them. However, no systematic search for such "secondary structures" (Louise, 1982, *Astronomy and Astrophysics* **102**, 303) is planned.

(d) High spectral resolution observations, with a spectral resolving power as high as 10^5 , in order to obtain accurate line profile leading to the expanding shell velocity determination, are still exceptional.

Our observing programme is derived from previous remarks. Indeed, we are now planning the "Monochromatic Atlas of PN". Monochromatic photographs must be made by using narrow interference filters ($\Delta\lambda = 10 \text{ \AA}$) centered on $H\alpha$, $H\beta$, $[\text{NII}] \lambda 6584$, $[\text{OI}] \lambda 6300$, $[\text{OIII}] \lambda 3727$, $[\text{OIII}] \lambda 5007$ and $[\text{SII}] \lambda 6717$. In order to access to photometric measures, each plate must be accurately calibrated. For northern PN an observing programme is engaged since 1981 by using the F/6 Newtonian focus of the 1.2 m telescope at the Haute Provence Observatory (OHP). A sample of preliminary results is given in Fig. 1 (a, b, c) showing NGC 7048 respectively in $H\alpha$, $[\text{NII}]$ and $[\text{OIII}]$ lines. Fainter PN must be observed with modern receivers such as the photon-counting system. Fig. 2 shows A 76 in the $H\alpha$, $H\beta$ and $[\text{NII}]$ lines. As for southern PN, observations are foreseen at the 1.54 m Danish telescope coupled with the CCD camera at La Silla.

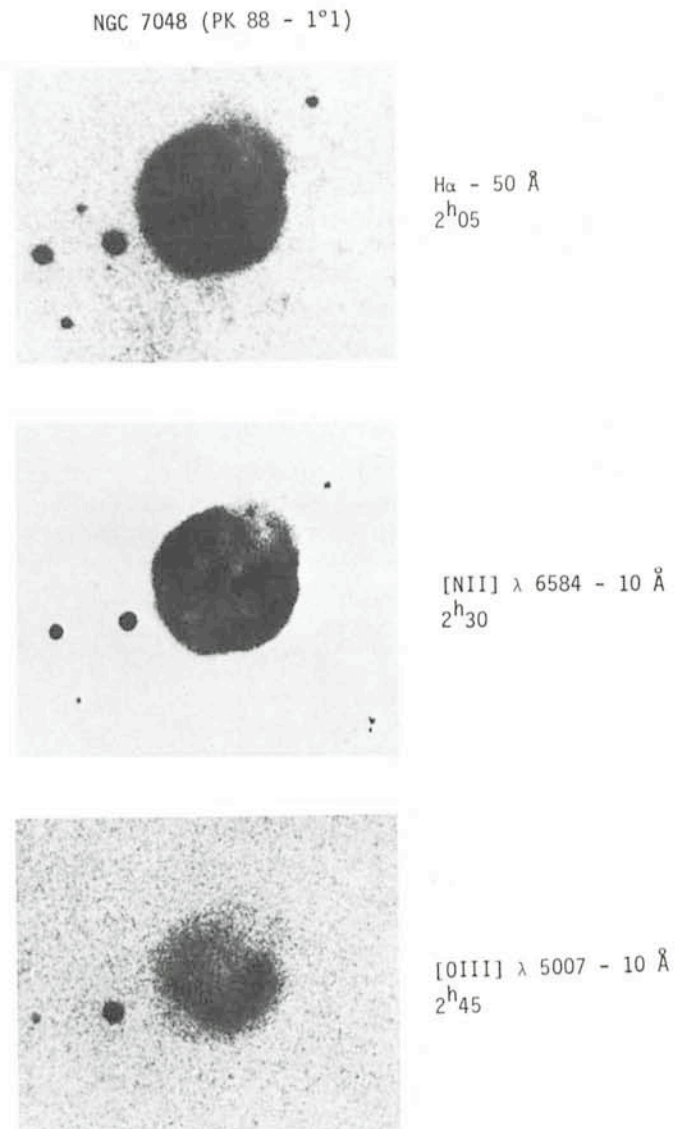


Fig. 1: Monochromatic photographs of NGC 7048 obtained with the 1.2 m telescope of the Haute-Provence Observatory.

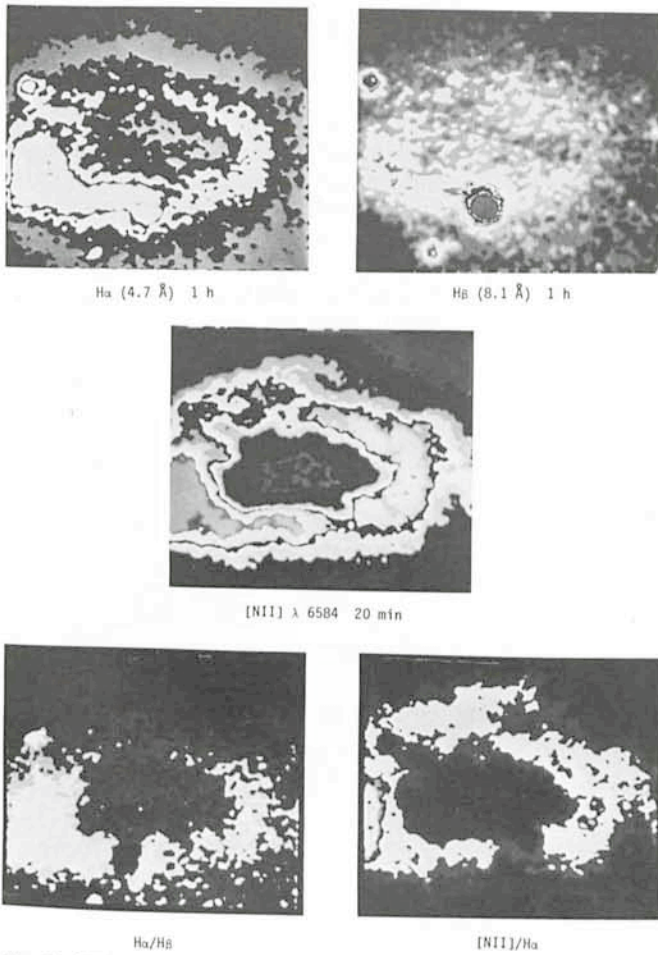


Fig. 2: A79 observed with a photon-counting system.

The Use of Monochromatic Plates

Monochromatic plates lead to the following data:

(1) Isophotic contour maps in an arbitrary scale are constructed for each observed line. The absolute scale may be obtained by using absolute spectrophotometric measures of one or more "connecting points" for a given nebula.

(2) Morphology and ionization structure of O^0 , O^+ , O^{++} ions as well as N^+ and S^+ ions are directly seen in monochromatic plates.

(3) As pointed out by Louise (1974, *Astronomy and Astrophysics* 30, 189) ring PN are either a result of the shell projection on the plane of sky or a toroidal main structure. Monochromatic observations combined with high spectral resolving power observations obviously lead to an accurate geometrical model (Louise et Maurice, 1982, *The Messenger*, 28, 28). Such a model can tell us about the formation and evolution of some ring PN (Louise, 1981, *Astronomy and Space Science* 79, 229).

(4) Ratios of different emission lines derived from monochromatic plates are available for drawing contours of equal ratio-lines (Hua et Louise, 1982, *Publications of the Astronomical Society of the Pacific* 94, 453). Usual important line ratios connected with physical properties of PN are as follows:

(a) Isothermal contours are derived from the $I(4363)/I(5007)$ of the [OIII] lines (Louise, 1981, *Astronomy and Astrophysics*, 98, 81).

(b) Internal dust distribution is revealed by $H\beta/H\alpha$ ratio variation from point to point.

(c) Iso-density contours are given by $I(6730)/I(6717)$ of the [SII] lines.

(d) Stratification structure of oxygen atoms is derived from combined ratios of [OI], [OII] and [OIII] lines.

Systematic Search for Faint Nebulosities

Long exposure plates using classical or/and modern cameras not only reveal faint nebulosities associated with PN but also detect new faint nebulae. In a next paper, Louise et Maurice will discuss about the detection of three faint nebulae located within 3 arcmin at the N-E side of NGC 1714 during their recent observing run at the 1.54 m Danish telescope coupled with the CCD camera.

Following our observations made at both OHP and ESO at La Silla, it seems likely that outer fainter halos around classical PN may be common. This result has implications on the total mass ejected from the PN progenitors, and possibly on the origin of the nebula (Terzian, 1982, *IAU Symposium* 103, final review).

Spectrophotometric Observations

Obviously, monochromatic plates can lead only to relative photometric measures. In addition, classical plates are less accurate than modern electronic receivers. Nevertheless, Hua et Louise (*Publications of the Astronomical Society of the*

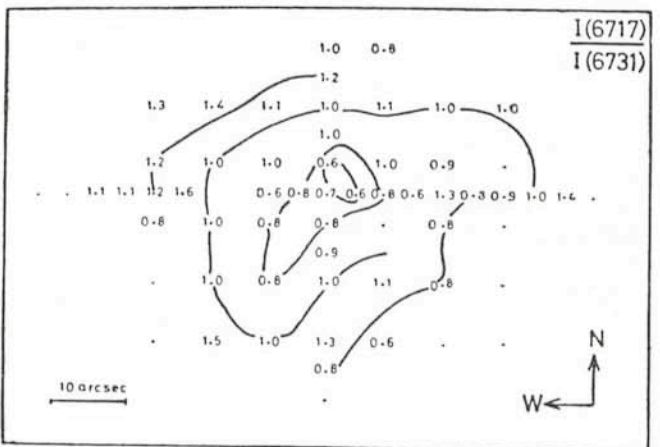
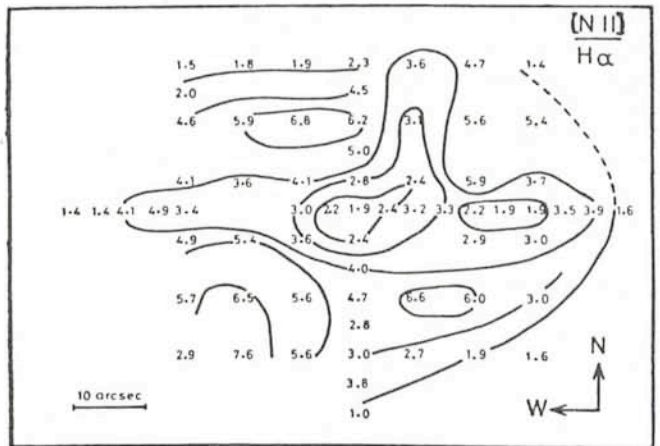


Fig. 3: NGC 2440. Upper panel: map of the ratio $I([NII] \lambda 6584)/I(H\alpha)$. Lower panel: map of the ratio $I(\lambda 6717)/I(\lambda 6731)$ of the intensities of the [SII] lines. From observations with the Image Dissector Scanner attached to the ESO 1.52 m telescope.

Pacific 94, 453) pointed out the possibility of using combined classical plates and modern devices. The procedure they proposed has the simplicity of classical plates and the photometric accuracy of modern cameras. This procedure will be used throughout when making up the "Monochromatic Atlas of PN".

For southern PN the IDS system will be used extensively in order to obtain spectra from point to point over the whole image of the nebula. We give in Fig. 3 a preliminary result on a peculiar nitrogen-rich nebula NGC 2440. The observations were made with the 1.52 m ESO telescope using the B & C spectrograph with a 4" × 4" entrance slit and a spectral dispersion of 59 Å/mm. We have obtained more than 65 spectra covering the whole image of NGC 2440. Contours of I(6717)/I(6731) of the [SII] lines shown in Fig. 3 reflect the

variation of the "skin density" within the nebula, because [SII] lines are originated only from low-excitation part of the filamentary structure of NGC 2440.

Conclusion

Monochromatic photographs in various emission lines and extensive spectrophotometric measures are complementary data which increase our knowledge about both morphological and physical structure of PN. Filamentary structure, globules, faint halos, etc. are the consequence of the evolution of these fascinating objects. There are so many physical and stellar processes occurring within the expanding shell! Routine but accurate observations foreseen for our Atlas will tell us more about expected and unexpected features of PN.

The Bright Star Catalogue Complete in Radial Velocities

J. Andersen and B. Nordström, Copenhagen University Observatory, Denmark

In many investigations, it is desirable to have certain observational data available for all stars of a given group, all over the sky, but – alas – reality is often far from this ideal. If you are an observing stellar astronomer, you have probably heard the reproach that "even in the Bright Star Catalogue, there are still xx stars without . . .", and it is true that even for the 9,000 brightest stars many basic data are still missing.

One kind of such data is (was) radial velocities. A few years ago there were still some 1,500 HR stars with no radial velocity determination at all – only 12 of them in northern declinations. At the same time, uvby β photometry had become available for all HR stars to spectral type G0, with Geneva photometry in progress for the rest. Radial velocities were needed in order to include kinematics in the astrophysical discussion of ages, metal abundances, etc.

So, we decided to do something about it, and we are happy to report that after our final observation on September 28, 1982, all stars in the Bright Star Catalogue should now have a radial velocity determination.

The ~ 800 HR stars later than F5 were observed with the CORAVEL scanner as part of the larger collaboration to use this instrument on the Danish 1.5 m telescope (Imbert and Prevot, 1981, *Messenger* No. 25, 6). The accuracy of CORAVEL is so high (about ± 0.2 km/s for bright stars) that just two observations per star, separated by a few months, are enough to detect most of the binaries. The speed and ease of observing with CORAVEL on a computer-controlled TV-equipped telescope was an experience we were well qualified to enjoy from the earlier part of the programme: With CORAVEL we could sit quietly and observe up to 17 stars per hour, results fully reduced – and no plates to develop and measure afterwards.

What a change from our 65 exhausting nights on the ESO 1.5 m coudé spectrograph, where we took some 3,000 plates of our ~ 800 early-type programme and standard stars! Unfortunately, CORAVEL cannot observe the early-type and/or fast-rotating stars, so the B–F4 stars had to be observed in the classical way. Even at 20 Å/mm, exposures are only about 5 minutes, and if you subtract the few nights that were too cloudy even for this kind of work, we took an average of about 50 plates per night, with a maximum of 89. To avoid losing time between exposures, ESO consented to our proposal for an observing team of two night assistants and two astronomers,

where everyone had their assigned jobs like setting the telescope, making the exposures, changing and making plates, and keeping the observing log.

This may sound like overstaffing, but if you take 3–5 minute exposures all night, everyone is really busy all the time, even too busy to eat a decent meal at midnight. Often we just had to grab some snacks as we went along – had you ever realized that it takes about five radial velocities to eat a fried egg? If you then count an additional four hours of darkroom work every afternoon, you may well guess that we were exhausted after our two-week runs. So, we are sure, were all our devoted night assistants who raced back and forth all night with great enthusiasm. We trust they will be rewarded with a long life in strong health from all this physical exercise, and thank them all again for their efforts.

But our work only began when the plates had been taken: Using an oscilloscope measuring engine constructed with the kind help of ESO and the Munich Observatory, the plates still had to be measured, a much larger job.

Our two first catalogues of new velocities have just been accepted by *Astronomy and Astrophysics* together with a paper describing our standard star observations, spectral line selection where we have included specifically the problems caused by stellar rotation, variability criteria, etc. Let us just note here that the standard error for one plate turns out to be in the range 1.3–2.5 km/s, depending on rotational line broadening. Our mean velocities (from 3–4 plates per star) are thus quite good.

Although observations were still in progress and not all checks and calibrations were final at the time, we were happy to be able to supply some 700 new, preliminary radial velocities for the 4th edition of the Bright Star Catalogue, which has just appeared. We expect the remaining final data to become available towards the end of this year.

During the coudé programme, we came across many new interesting stars: If a star has no radial velocity determination, it was possibly never observed at high dispersion before. E.g., among the 50 or so new double-lined binaries we found in all, some 6 were subsequently discovered to be eclipsing, and we have now observed complete light curves and spectrographic orbits for them. One of them is TZ For (HD 20301), which is the only known double-lined eclipsing system with two normal G giants. Its long period ($P = 75.7$ days) has led to a collaboration

between many photometric and CORAVEL observers in order to complete the data.

Another unusual acquaintance was the pre-main sequence star HR 5999 (see Thé and Tjin A Djie, *Messenger* No. 16, 33, and 23, 25): One night, we suddenly found ourselves exposing for over half an hour on a programme star! Clearly, something quite exceptional must be happening, and, indeed, until very recently ours were the only plates taken at a deep photometric minimum. From them, it was possible to detect differences

between the circumstellar dust and that in normal interstellar matter (*Astronomy and Astrophysics* 113, 176). The B-type visual companion HR 6000 shows a variety of bizarre abundance anomalies which we are studying more closely at present.

So, although our programme – like many others – involved a large amount of routine work, there was a sprinkling of spices to sustain the appetite. But, of course, we still hope that our results for the 95% normal stars will also be found useful.

Envelopes Around Carbon Stars

First Spectrophotometric Observations with the New Infrared Photometer at the 1 m Telescope

P. Bouchet, ESO

Introduction

The new infrared photometer was installed and checked at the 1 m telescope for the first time in June 1982. However, the software facilities being not fully operational, it was then impossible to test it on astronomical observations. The first successful observations with this system were carried out in December 1982. Despite poor weather conditions, some interesting results could be obtained in the spectrophotometry mode, which make this new facility very attractive and worthwhile to be reported as an example of what can be achieved.

Observations

The photometer is mainly similar to the one used with the 3.6 m telescope. It has been described by A. F. M. Moorwood in *The Messenger* (No. 27, March 1982). It was used for these first tests with a bolometer equipped with a circular variable filter (CVF) covering the 8–14- μm region at a resolving power ≈ 100 .

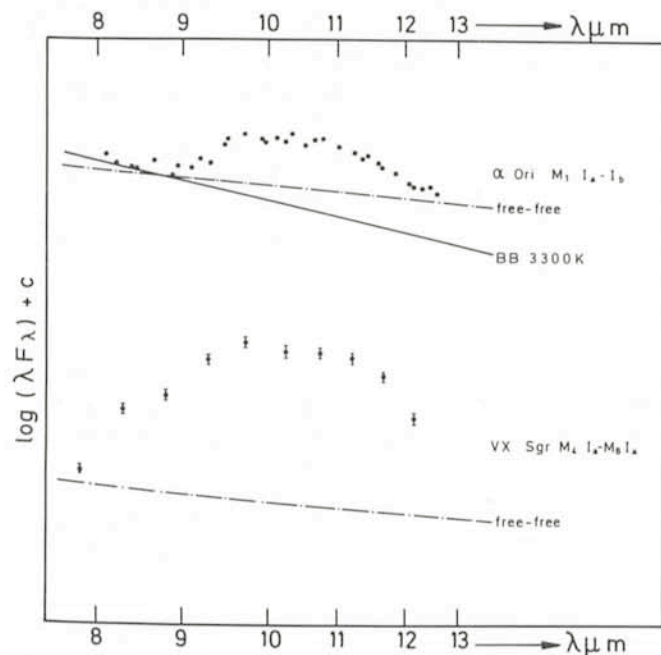


Fig. 1: Spectrophotometry of representative supergiants showing the 9.7- μm silicate emission band. A 3300° K blackbody and an ionic free-free slope, as suggested by R. C. Gilman, 1974 (*Astrophysical Journal*, 188, 87), are included for comparison.

The principal features readily recognized in that observed spectral range are the silicate band at 9.7 μm ($\Delta\lambda \sim 3 \mu\text{m}$) and the silicon carbide near 11.2 μm ($\Delta\lambda \sim 1.7 \mu\text{m}$). These two bands infer the presence of circumstellar dust envelopes in

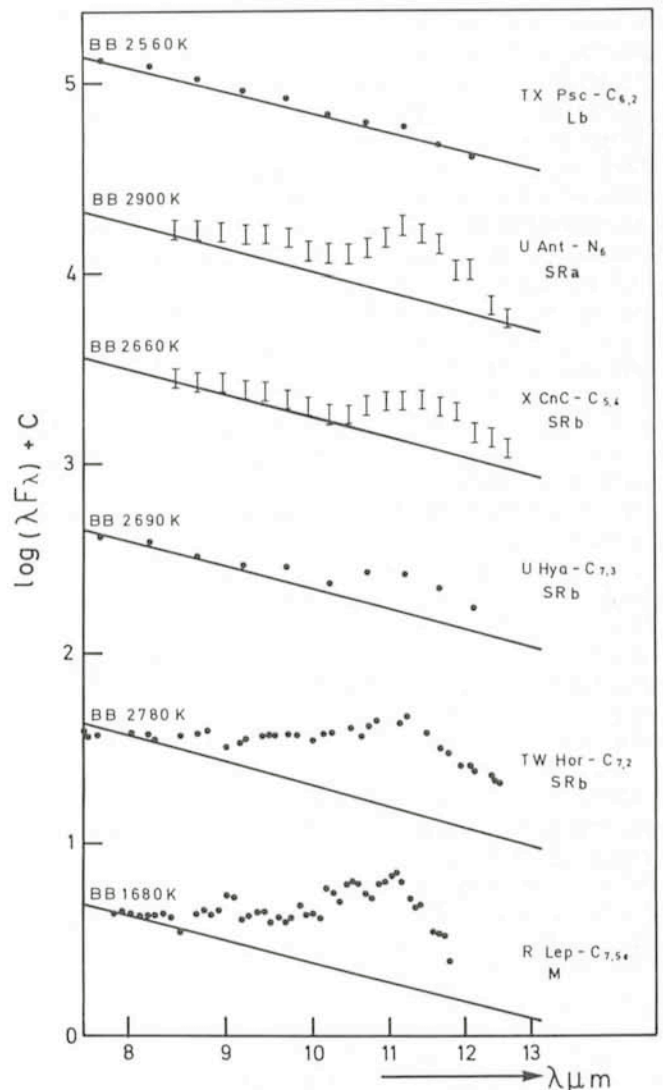


Fig. 2: Spectrophotometry of a sample of carbon stars, identified by their spectral type and type of variability. Note the dense dust envelope around R Lep and TW Hor.

late-type stars and have been extensively discussed by K.M. Merrill (IAU Symposium No. 42, Bamberg, 1977).

The observations were carried out during the nights of 4 and 5 December, 1982. The reductions have been made using the stars B1 Ori (spectral type C6.2; $T_e = 2670^\circ\text{K}$) and TX Psc (spectral type C6.2; $T_e = 2650^\circ\text{K}$) as standards. Both stars are known to lack an envelope and to show no infrared feature in the spectral range observed. The results are shown in Figures 1 and 2. When no error bar is given, the internal accuracy is roughly equal to the size of the plotted points. In 1-min integration time, the signal-to-noise ratio achieved for R Lep ($N = -2.5$) was approximately 100.

The silicate emission band is seen in oxygen-rich stars. Fig. 1 shows the relative $\lambda\lambda$ 8–13- μm spectrophotometry of two representative M supergiants, α Ori and VX Sgr. The silicate emission band is clearly seen in α Ori and very strong in VX Sgr, which are well-known results.

The silicon carbide band is seen in carbon-rich stars. The fundamental constituent of the dust in the envelope of these stars is relatively featureless (Forrest et al., 1975, *Astrophysical Journal* **195**, 423) and is generally considered to be condensed carbon. That carbon is mixed with SiC, gaseous CO and other metallic molecules in an expanding envelope of which the principal indicator is then the emission due to the SiC.

Fig. 2 shows the relative $\lambda\lambda$ 8–13- μm spectrophotometry of a sample of carbon stars, together with the appropriate black-body slopes for each star. Some of the stars of the sample were already known to have an envelope (X Cnc, U Hya and the famous Mira variable R Lep). The detection of an envelope (X Cnc, U Hya and the famous Mira variable R Lep). The detection of an envelope around U Ant is new, however, as is the detection of a very dense one around TW Hor. This latter envelope deserves special mention regarding the controversy

on its reality, as discussed by P. Bouchet et al. in the same issue of *The Messenger*.

Two other carbon stars, not known to bear an envelope, were also observed and were not included in Fig. 2: W CMa (spectral type R_b, variability type L_b), which did not show any silicon carbide emission, and AB Ant (spectral type N_b, variability type SR_b), which does seem to show such emission. However, the S/N in the latter case is too small to lead to a definite conclusion.

Conclusion

Envelopes have been detected around the carbon stars U Ant and TW Hor and, probably, AB Ant, while the spectrum of W CMa does not show any SiC signature. The existence of envelopes around X Cnc and U Hya has been confirmed, and our results for the M supergiants α Ori and VX Sgr and the carbon-Mira R Lep reproduced perfectly those obtained by Merrill (1977) and previous observers.

These results should give a good notion about the exciting new infrared facilities offered henceforth at the 1 m telescope on La Silla. It should also be emphasized that these observations were made during the first observational test of the equipment and, as such, the signal-to-noise ratio achieved in our measurements should further improve in a very near future, when the system becomes thoroughly operational. Special thanks should be given to the ESO staff in Garching who made the project a reality, namely A.F.M. Moorwood and A. van Dijsseldonk, and the technical staff at La Silla, especially J. Roucher and F. Gutiérrez, who assisted and helped me with their active efficiency during these first tests. I would like to thank also Miss Victoria Tapia who made the drawings.

Chemical Composition in the Small Magellanic Cloud

R. Foy, Observatoire de Calern

The Magellanic Clouds are the two nearest galaxies; the well-known great Andromeda Nebula M31 is about ten times farther away than the clouds. They are much smaller than M31, but their nearness justifies the large amount of observations devoted to them, particularly at La Silla. They provide us the best suitable tests at least for two fields of theoretical astronomy.

The first one concerns models describing the evolution of the mean chemical composition in a galaxy. The nuclear reactions which produce the energy radiated by stars lead to the synthesis of heavy elements (i.e. heavier than helium). Part of these heavy elements are then ejected in the interstellar medium by way of stellar winds or novae or supernovae explosions. Then the enriched interstellar matter is recycled to form a new generation of stars. This behaviour is modelled as a function of various parameters. The total mass of the galaxy, and the ratio of the mass of the interstellar gas to the mass condensed in stars are two major parameters in these models. The large and small clouds have different masses, 6×10^9 and $1 \times 10^9 M_\odot$ respectively, which is small compared to the mass of our galaxy (about $150 \times 10^9 M_\odot$).

The ratio mass of interstellar gas/mass of stars is also different (5 per cent in the LMC, and 30 per cent in the SMC). Therefore, models of chemical evolution of galaxies can be applied to two very different objects which are also very

different from our galaxy. Obviously a crucial check for these models is to compare the predicted chemical composition with the observed one.

Before discussing how the chemical composition in the clouds can be determined, let us briefly mention the second main interest of the clouds: the kinematical interaction between galaxies. The clouds are gravitationally linked to the Galaxy. Tidal effects due to the large mass of the galaxy are expected to be a major factor in the dynamical and kinematical evolution of the clouds, at least when the "first close encounter" between the clouds and our galaxy occurred, presumably, 1 to 3×10^8 years ago. Observational tests in this field are the determination of the three-dimension morphology of the clouds, which is still much debated, and the study of the velocity field distribution, from radial velocity measurements.

(A) From Which Objects Can We Determine the Chemical Composition?

Traditionally, chemical compositions are determined from high-dispersion stellar spectra, but another interesting way is the spectroscopy of bright gaseous nebulae: H II regions, planetary nebulae or supernova remnants.

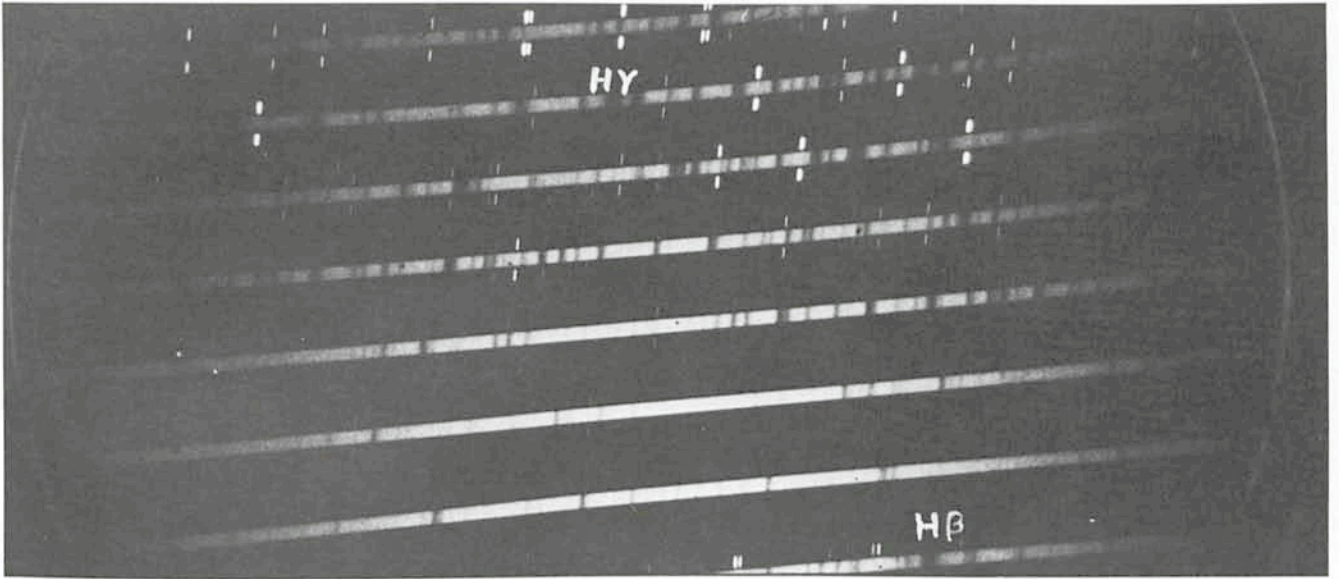


Fig. 1: Spectrogram of the SMC supergiant AZ369, obtained with the Echelec spectrograph and the electronographic camera at the 1.52 m ESO telescope. The reciprocal dispersion on the original is about $9\text{\AA}/\text{mm}$, depending on the order. The exposure time was 8 hours 21 minutes, with a seeing of $2''$ (entrance slit: $1.3''$) and a good transparency.

1. The Stars

Observations of stars in the SMC are quite delicate:

- They are remote objects, more than 200,000 light years distant. Stars of which the chemical composition is usually determined lie in the solar neighbourhood, at a distance from the sun 100 times smaller.

- The brightest stars in the SMC are intrinsically fainter than in the LMC (at a distance from the sun smaller by about 15 per cent) roughly by one magnitude.

- The surface density of stars in the direction of the clouds is very high, implying a risk of contamination of the observed spectra. The brightest stars, i.e. the easiest to observe, are supergiants. This adds another difficulty to the interpretation of their spectrum in terms of atmospheric physical parameters. This difficulty is illustrated as follows: The brightest star in the SMC HD 7583, with a magnitude $M_v = 10.1$, has been studied by Przybylski and also, at La Silla, by Wolf. The first found that metals in this star are ten times less abundant than in the sun, whereas the second found that its chemical composition is not significantly different from the solar one; but Dubois, using low-dispersion spectrograms obtained with the 1.52 m ESO telescope, has shown that spectral lines of this exceptionally bright supergiant are variable.

Using the same telescope, with the Echelec spectrograph and the Lallemand-Duchesne electronographic camera, I have observed four stars expected to be "normal" cool supergiants in the SMC on the basis of photometric and low dispersion spectrographic data. I have chosen supergiants not extremely bright and relatively cool (with roughly solar temperature) to have less severe problems in the interpretation of the spectra. Magnitudes range from 11.1 to 13.3 in the visible: Add about 0.6 to 0.7 magnitude to obtain the magnitudes in the blue, the spectral range in which the observations were carried out.

High dispersion spectroscopy of such faint stars at the coudé focus of a moderate size telescope is quite difficult. Identification of stars in the small but crowded field of the coudé focus is sometimes not simple. Exposures were very long, up to more than 9 hours, and had to be done in complete darkness, because of the high sensitivity of the detector. How many times the night assistant and I must have shouted to visitors in the coudé room: "No luz, no luz . . ." (and ". . . por favor" at the beginning of the night)? Guiding also was hard.

I obtained good quality high-dispersion spectrograms (see Fig. 1). This was possible thanks to the staff of the electronographic camera at La Silla (J. Breysacher at the beginning, then P. Giordano and A. Torreron) who prepared the cameras with great care. It is a pleasure for me to thank them here again.

I performed the analysis of the spectrograms at Meudon. One star turned out to be a galactic giant on the line of sight of the SMC; the three others are really SMC members. One of them is completely analysed (Foy, R. 1981 *Astronomy and Astrophysics* **103**, 135): It is AZ369. Except for HD 7583, it is the only star which has been analysed in detail in the SMC. I found that metals are moderately deficient with respect to the solar abundances: There are 2.5 times less metals in this star than in the sun. From the present state of the analysis of the two remaining stars, I think that the metal abundances which I shall derive very soon will not be significantly different. This moderate deficiency of metals in stars is confirmed by low-dispersion spectroscopy of F supergiants and of RR Lyrae type variables.

2. The Bright Gaseous Nebulae

Interstellar matter is bright around stars able to excite the gas, or on the front of shock-waves. In H II regions, the gas is excited by one or several very young hot stars. Due to the large volume concerned, the total luminosity of an H II region is high, so that it is possible to observe this kind of objects in remote galaxies. A lot of work on emission lines in H II regions in the SMC was done with the 4 meter Anglo-Australian telescope by Pagel and collaborators. They found that oxygen is deficient by almost a factor of 10, and nitrogen by a factor of 40 with respect to the sun. This extra deficiency of nitrogen is well accounted for by models of chemical evolution of a galaxy. Nitrogen would be a second-generation element, extremely deficient, if existing, in the matter of the proto-galaxy from which the SMC was born.

Similar results are obtained from the analyses of planetary nebulae spectra, the circumstellar components of the remnant of a nova explosion.

The unique supernova remnant analysed in the SMC also reveals a marked deficiency in nitrogen with respect to oxygen, but no firm value is proposed for the oxygen abundance.

(B) What is the Chemical Composition in the SMC?

The discrepancy between the abundance determinations either from detailed analysis of stellar atmospheres or from studies of emission spectral lines in nebulae would not be as large as it seems. Indeed, in the first case, abundances of elements such as titanium, chromium, iron, calcium are determined, whereas the emission spectrum of nebulae leads to the determination of the abundance of helium, oxygen, nitrogen, sulfur, argon, and sometimes chlorine. These last elements could be slightly underabundant with respect to the iron peak elements. What does it mean, if it is significant, and if the abundance of iron in AZ369 is representative of the iron abundance in the recently synthesized material in the whole

SMC? Light elements, like oxygen, are mainly synthesized in massive stars, and iron peak elements originate from type 1 supernovae, of which progenitors are less massive stars. Therefore the ratio of the number of massive stars to the number of intermediate mass stars would be smaller in the SMC than in the solar neighbourhood. The initial mass function would be steeper in the SMC than in our galaxy.

Thus, what to do to achieve further progress?

Try to derive the oxygen abundance in stars, which is difficult, or to observe fainter stars, so that problems in the interpretation of the spectrum are much less severe. We hope to do that with the new CASPEC spectrograph at the 3.6 m telescope at La Silla.

MIDAS — ESO's New Image Processing System

*K. Banse, P. Crane, P. Grosbøl, F. Middleburg, C. Ounnas, D. Ponz and H. Waldthausen
Image Processing Group, ESO-Munich*

Introduction

In 1979 ESO began the planning and development of a new image processing system to fulfill the data analysis and image processing needs for the 1980's. It was decided to use a powerful 32-bit super-mini computer with virtual memory management as the basis for this development. The VAX 11/780 computer of Digital Equipment was chosen mainly because of its user-friendly operating system, VMS, and because the VAX had been selected by several other astronomical institutes. Indeed, the STARLINK system in the U.K. and the FIPS system developed at ESTEC for the Faint Object Camera are based on VAXes.

Soon after ESO's move to Munich, the first VAX 11/780 was installed and the actual development began. The software system was given the name "MIDAS" which stands for **Munich Image Data Analysis System**. In mid-1981, the image display systems were delivered, and in late 1981, the second VAX was installed. The developments progressed to the state where local users began using the MIDAS system in early 1982 and they have reached the state where outside users are being encouraged to use the system for analysing CCD data; however, at the present time the reduction package is not totally completed. Of course, the range of applications of MIDAS is growing rapidly beyond the CCD.

In addition to developing MIDAS for use at ESO in Munich, some effort has been put into making the system easy to transport to other VAXes with different graphics and image peripherals. A copy of MIDAS will be installed on La Silla soon after the VAX arrives.

Hardware Elements

The hardware configuration of MIDAS in Munich is shown in Fig. 1. The important components are the VAX CPUs with their associated disk and tape subsystems, the image display systems, and the Dicommed image recorder.

The heart of the system is the two VAX 11/780 computers linked together via DECnet. VAX-A is equipped with 3.5 Mbytes of memory, 1.2 Gbytes of disk storage and 2 tape drives with 800/1600 bpi density. VAX-B has 4.0 Mbytes of memory, 688 Mbytes of disk storage and one tape drive with 1600/6250 bpi density.

The philosophy behind the disk and tape arrangements was to enable users to keep an important quantity of their data on disk while they are actively reducing it and only to use tapes at the beginning and end of their work.

The image display systems used for MIDAS in Munich are 3 Gould-DeAnza IP-8500 systems. Each system is equipped with a powerful Digital Video Processor (i.e. an array processor processing entire frames of 512*512 pixels at video rates), and supports two user stations with each station having its own cursor and overlay. Currently each station has 4 image channels and 1 overlay channel of 512*512*8 bits each, as well as an alpha-numeric memory of 20*80 characters. Two of the IP-8500 systems are connected to VAX-A and one to VAX-B.

The DeAnza system of VAX-B includes also a video digitizer system connected to a TV camera. This system allows pictorial and graphical data to be entered quickly into the computer for making overlay and so forth.

The Dicommed image recorder serves as a high resolution hardcopy device for publication and reference. The output is normally on regular roll film and is of excellent quality. Fig. 2 shows an example of some output from the Dicommed.

In addition, a Versatec plotter is connected to each VAX. An HP plotter is also available on VAX-A.

The MIDAS work station is very similar to the one of IHAP. Each of the six MIDAS work stations consists of a DeAnza display, a VT100 terminal for command input and data in/output, and an HP 2648 terminal for graphic output. However, MIDAS procedures which do not require the interactive peripherals can be run from any terminal connected to the VAX. Output to the Versatec, HP Plotter and Dicommed is spooled like output to the printer.

The MIDAS Software Environment

The design of MIDAS was influenced by the following factors:

- The system should be compatible with the other major astronomical image processing systems which are currently developed, i.e. Starlink of Rutherford Appleton Laboratories in England, the Faint-Object-Camera Image Processing System of ESTEC in Holland and the system for the Space Telescope Institute in Baltimore.

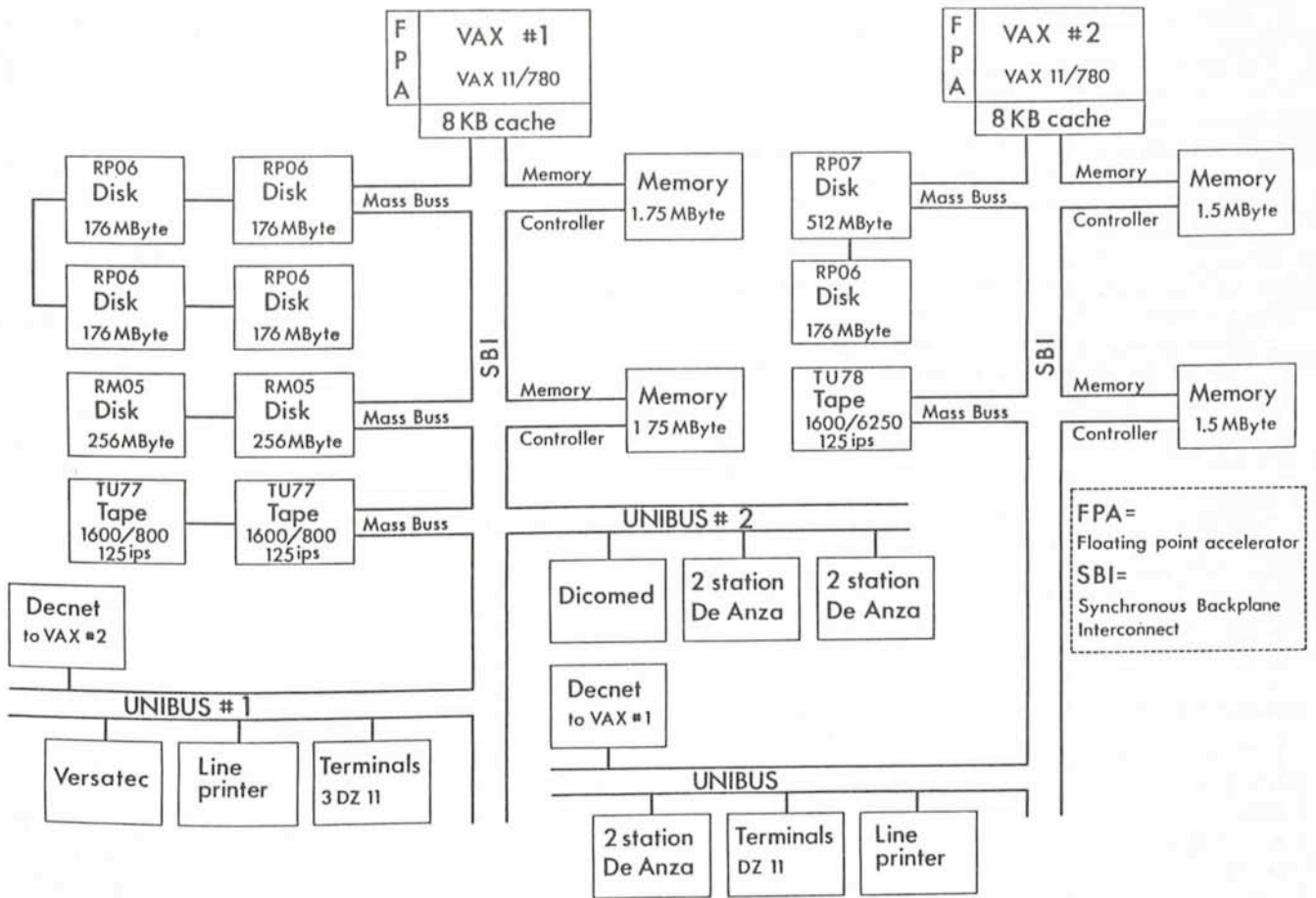


Fig. 1: The hardware configuration of MIDAS.

- The experience and insight gained with the highly successful IHAP, ESO's current Image Processing System based on HP 1000-F computers, should be used.
- MIDAS will be used heavily by visitors, thus it should be quick and easy to learn the basic features of the system.
- A modular system with simple interfaces to data structures, e.g. images, is required to facilitate implementation and conversion of existing application software from other institutions.

The above considerations led to an implementation of MIDAS with the following features:

- Like IHAP it is a command-driven system geared towards the interactive user. The structure and syntax of MIDAS commands has been modelled after DCL, the command language used on the VAX with the VMS operating system. A command line may be up to 200 characters long and is structured as

command/qualifier par1 par2 . . . ! comments.

The "command" describes the general action to be performed (an English verb) and the qualifier specifies how to perform the action (an adverb). For example, the command: WRITE/KEYWORD KEY DATA stores "DATA" into the "keyword", named KEY.

- The type and number of parameters in a command depends on the particular command invoked. The parameters are position-dependent, but this can be overridden.
- An extensive on-line help facility provides detailed descriptions of all commands and qualifiers.
- MIDAS is a very modular system that provides building blocks for making more sophisticated applications. In fact, most of the "commands" are not commands at all, but MIDAS procedures which are a series of "commands" linked

together with control structures to perform the desired operation.

- Conditional branching, nested looping, local/global variable substitutions and calls to other procedure files are features of a MIDAS command procedure.

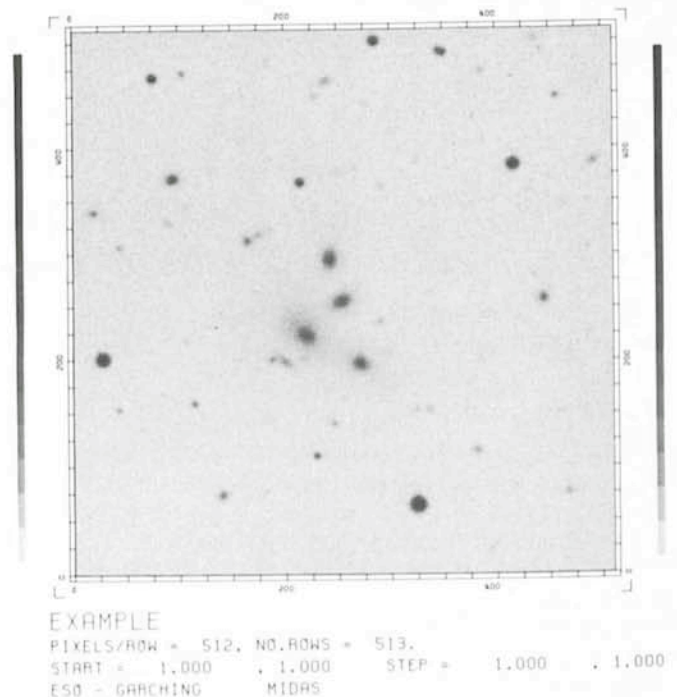


Fig. 2: An example of some output of the Dicomed image recorder.

- MIDAS supports several data structures. These are outlined below:
 - Images, a collection of data of the same physical significance (cf. IHAP).
 - Tables, data which can be arranged in rows and columns and not necessarily of the same physical significance. Tables are extremely useful in handling the results of various operations such as lists of magnitudes.
 - Descriptors, the information which is associated with images or tables. These would typically be the name of an image and the number of pixels on each axis as well as many other things.
 - Keywords, variables which provide communication between different MIDAS application programmes. For example, the position of the cursor is normally stored in a keyword and then passed to a subsequent application programme.
- Input to MIDAS is either via the terminal keyboard or from ASCII files, which are the MIDAS command procedures. These files may contain any supported MIDAS command but also the control structures similar to those of high-level programming languages.
- MIDAS users keep a reasonable amount of their data on disk during the time they wish to work. Thus no time is lost in moving data from magnetic tape to disk and vice versa. For this purpose, several "public" disk areas of various sizes have been established for which a MIDAS user can obtain exclusive access for a certain time.
- Two commands have been created to read and write magnetic tapes. These procedures support IHAP, FITS and DEC's BACKUP format on input as well as FITS and BACKUP on output.
- Single images may be viewed in monochrome or with pseudo colours. If the 3-colour components of an image exist, they may be overlaid to work in real-colour mode (cf. Fig. 2, page 27 in *Messenger* 30, Dec. 1982).
- Extract subimages interactively via cursor window or at fixed coordinates.
- Plot scan lines, contours and perspective views.
- Rotation, flip, rebin and filter images.
- Execute arithmetic operations and the usual FORTRAN functions on images and tables as well as Fast Fourier transformations.

It is envisaged that several application programme packages will be developed within the MIDAS environment. These will function and be documented along the lines of the IDS reduction package that has been available in the IHAP system for several years.

The first astronomical application package implemented in MIDAS handles CCD frames. The CCD images are cleaned by minimizing permanent instrumental defects, such as low sensitivity columns, bad rows and hot spots and by removing various kinds of random artifacts. In its present state, MIDAS will be most useful for astronomers wishing to reduce CCD data.

Other astronomical applications in the areas of 2D-photometric and spectroscopic reductions are currently being developed for MIDAS and will be fully integrated soon.

Documentation

An extensive users guide has been written which describes the MIDAS system as it currently exists and how to use these features. As new features are added, the users guide will be updated. This includes descriptions of the data structures, detailed descriptions of the individual commands, and information on how to use the special-purpose peripherals such as the Dicomed image recorder.

A guide to writing an application programme for the MIDAS system is also available. It describes the FORTRAN interfaces to the MIDAS data structures. This will prove useful to those people who wish to generate special-purpose commands for their own particular application.

Finally, a MIDAS installation guide and MIDAS system description have been written, but their status is less well developed than the previous two.

Applications

At the present time MIDAS provides a comprehensive set of basic image processing functions. There are currently about 175 commands available in the MIDAS system. A short overview of the most interesting ones is given below:

- Load images and colour-lookup-tables into the image display and read them back into VAX memory.
- Modify the colour-lookup-table interactively to enhance various image features.
- Zoom and scroll images interactively or with fixed values.

Absorption-Line Spectroscopy of Close Pairs of QSOs

P. A. Shaver, ESO, and J. G. Robertson, Anglo-Australian Observatory

Introduction

QSOs can be used as sensitive probes of the intergalactic medium. They are strong and distant sources of continuum radiation, against which intervening material may be discerned in absorption and mapped as a function of redshift. Close QSO pairs, which by chance have small separations (\leq few arcmin) on the plane of the sky, expand these possibilities; they provide twin lines of sight over vast distances, giving direct information on the lateral sizes of the intervening absorbing regions distributed along these lines of sight, and on the presence of absorbing material in the immediate vicinity of the foreground QSOs themselves.

Two distinct types of absorption lines are found in QSO

spectra. There are broad absorption troughs adjacent to the emission lines in about 10 per cent of QSO spectra; these are high-excitation systems, and are thought to be due to gas which has been expelled from the QSO nuclei. The origin of the other type of QSO absorption lines is more controversial: narrow absorption lines (widths of a few hundred km s^{-1} or less) are found in most QSO spectra, with any redshift up to approximately that of the QSO. They could conceivably also be due to matter which has been expelled from the QSO at highly relativistic velocities, but the most widely accepted view is that they are due to matter cosmologically distributed along the line of sight to the QSO and unassociated with it. These in turn fall into two categories: systems containing heavy-element

absorption lines in addition to Ly α , and the far more numerous systems in which only Ly α is detected and which comprise the so-called "Ly α forest" of absorption lines shortward of the broad Ly α emission line of the QSO.

What types of intervening objects could cause the narrow absorption lines? For the heavy-element absorption-line systems – possibly protogalaxies, spiral galaxies or large (100–200 kpc) galactic halos. If, as has been suggested, many of the Ly α absorption lines do not have heavy-element absorption-line counterparts (to very low levels), they would be due to comparatively unprocessed material, perhaps intergalactic hydrogen clouds (~ 10 kpc), or extremely large hydrogenic halos around galaxies or clusters of galaxies.

Direct evidence that at least some narrow heavy-element absorption lines originate in the extended halos of intervening galaxies has been obtained in a few cases in which absorption is seen at the redshift of a galaxy close to the QSO on the sky but with $z(\text{gal}) \ll z_{\text{em}}(\text{QSO})$. In almost all of these cases, the absorption lines are Ca II or Mg II, and the redshifts are relatively small. Indirect evidence further suggests that high excitation absorption lines of high redshift may also be due to intervening galactic halos: the detection of C IV absorption arising in the outer halo of our own galaxy, and statistical studies of high-redshift C IV absorption lines.

By looking for "common absorption" in close QSO pairs, i. e. absorption in both spectra at the same redshift, one may obtain more direct information on the nature of narrow absorption

lines of high excitation and redshift: evidence regarding their origin (intrinsic vs. intervening), and the sizes and clustering of the absorbing regions.

One may also look for "associated absorption", i. e., absorption at the redshift of the foreground QSO in the spectrum of the other member of the pair. This would give information on the clustering of absorbing material with QSOs and on the presence and nature of gaseous halos surrounding QSOs (which may be expected, if QSOs are the nuclei of galaxies). It would also address the intrinsic/intervening question of origin, and provide a new test of the cosmological interpretation of QSO redshifts.

Observations: Prospects and Results to Date

There are several suitable pairs listed in published catalogues. For every 100 QSOs, there is roughly one pair of separation ~ 1 arcmin with both members brighter than 20th magnitude. The number of such pairs is consistent with a random distribution of QSOs on the sky, and can be expected to increase rapidly as the vast amount of presently unpublished objective prism material becomes generally available. The advent of the Space Telescope will make still more pairs accessible to this kind of study. Gravitational lens pairs are of special interest in studying common absorption at very small angular separations, but the number of these is expected to remain small. Physical pairs of QSOs are also useful because

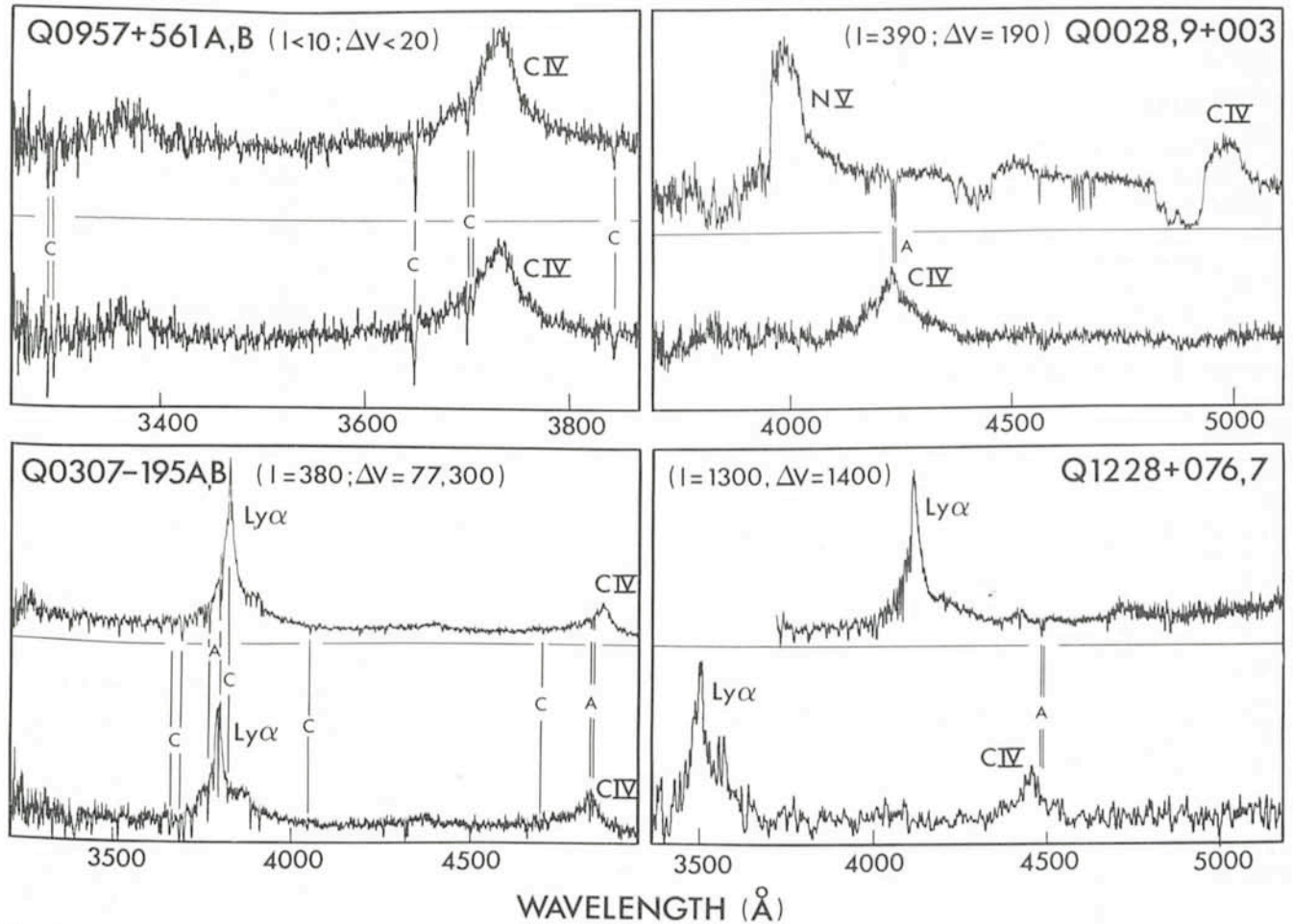


Figure 1: Spectra of four QSO pairs, showing common (C) and associated (A) absorption. Also indicated are the projected separation (l , in h^{-1} kpc) and the velocity difference (ΔV , in km s^{-1}). References are as follows: Q0957+561 A,B (Young et al. 1981, *Astrophysical Journal* **249**, 415), Q0307-195 A,B (Shaver and Robertson 1983, *Astrophys. J.* in press), Q0028,9+003 (Shaver, Bokseberg, and Robertson 1982, *Astrophys. J.* **261**, L7), and Q1228+076,7 (Robertson and Shaver 1983, *Nature*, in preparation).

of their small angular separations, but their small redshift differences may make them difficult to use unambiguously in studies of associated absorption.

Our programme of absorption-line spectroscopy of close QSO pairs, now just over a year old, involves the 3.6 m telescope at La Silla and the Anglo-Australian Telescope at Siding Spring. Both the IDS and the IPCS are used; a special advantage of using the IPCS for this kind of work is that both QSOs can be observed simultaneously, cutting integration times in half. We already have useful data on 8 QSO pairs, which, combined with data on a further 4 pairs observed by others, gives information on 20 heavy-element absorption systems for which common absorption could be detected and 11 QSO pairs in which associated absorption could be detected.

We have found several cases of associated absorption and a few of common absorption. The probability of any of these coincidences occurring by chance is small, about 1 per cent per QSO pair for a redshift coincidence of $\pm 200 \text{ km s}^{-1}$. This, therefore, provides the first direct evidence that at least some high-redshift absorption systems are due to intervening matter.

“Typical” Absorption Systems

Of the 20 heavy-element absorption systems found in the spectra of these QSOs and having much smaller redshifts than the QSOs themselves, only a few have definite counterparts in the spectrum of the other member of the pair (“common absorption”). Two of these occur in the gravitational lens pair Q0957+561A,B, for which the projected separations are very small. In the other case, Q0307–195A,B, the velocity difference is 297 km s^{-1} and the projected separation at the relevant absorption redshift is $376 \text{ h}^{-1} \text{ kpc}$ ($H_0 = 100 \text{ h km s}^{-1} \text{ Mpc}^{-1}$ and $q_0 = 0$). These cases are shown in Fig. 1. In view of the small incidence of common absorption, it therefore appears that typical heavy-element absorption systems may be no larger than several hundred kpc, and that, if they are clustered together at all, the absorption cross-sections of the clusters are small. Therefore, if the absorption systems are due to extended galactic halos, these results may provide constraints on the fraction of galaxies in clusters which can have such halos. By the same token it seems unlikely that the sub-structure found in these heavy-element absorption lines can be due to several galaxies clustered together, as has sometimes been suggested, unless the absorbing halos are very small. These inferences, however, must remain tentative until more data become available.

The Ly α absorbing regions are also not extended or clustered over very large scales. Sargent et al. (1982, *Astrophysical Journal* **256**, 374) found no significant correlation between the Ly α absorption lines in the spectra of the QSOs Q1623+268,9. The linear separation is $\sim 1 \text{ h}^{-1} \text{ Mpc}$ over the relevant range of redshift. In the Q0307–195A,B pair (separation $\sim 0.4 \text{ h}^{-1} \text{ Mpc}$) we found a marginal tendency for the Ly α lines to correlate, but more QSO pairs of separation $< 1'$ must be examined before firm conclusions can be drawn.

Absorption Systems Associated with Foreground QSOs

By contrast with the relatively few cases of common absorption, “associated absorption” (absorption in the spectrum of the higher-redshift QSO at the redshift of the other member of the pair) has been found in a comparatively large fraction of QSO

pairs. Some of these cases are shown in Fig. 1. Of all available QSO pairs (projected separations up to $2 \text{ h}^{-1} \text{ Mpc}$), half exhibit associated absorption, and for separations less than $500 \text{ h}^{-1} \text{ kpc}$ the fraction with associated absorption approaches three-quarters. Evidently QSOs are located in regions of high matter density – plausibly clusters of galaxies (which would then be the most distant known, with look-back times over half the age of the universe). The higher incidence of associated absorption (compared with common absorption) suggests that the absorption cross-section may be enhanced in the vicinity of QSOs; this is plausible since the UV flux from a typical QSO dominates the metagalactic flux over a radius comparable with that of a cluster of galaxies.

The very small velocity differences in the cases of Q0307–195A,B and Q0028,9+003, however, 77 and 190 km s^{-1} respectively, suggest that the absorption here may arise in extended halos or disks physically associated with the foreground QSOs themselves. Thus, we may be looking through one QSO at another. This interpretation receives strong support from the observations by Bergeron et al. (1983, *Monthly Notices of the Royal Astronomical Society* **202**, 125) of emission lines around the QSO MR2251–178 which extend out to at least $150 \text{ h}^{-1} \text{ kpc}$ and define a smooth rotation curve centred on the QSO redshift. The absorption measurements are sensitive to smaller column densities, and show that such halos may extend out to $400 \text{ h}^{-1} \text{ kpc}$. If this interpretation is correct, it implies that a large percentage of QSOs possess Mpc-diameter halos.

The nature of these halos remains uncertain at present, but the example of MR2251–178 does suggest a disk-like geometry. If these halos really are the quiescent disks of the parent galaxies containing the QSOs, the implied masses of the disks and the total systems are $\geq 10^{10} M_\odot$ and $\geq 10^{12} M_\odot$ respectively.

Cosmological Interpretation of QSO Redshifts

The discovery of associated absorption in close pairs of QSOs opens the way to a new test of the cosmological interpretation of QSO redshifts. According to the cosmological interpretation the foreground QSO in a pair should always have the lower redshift. On the other hand, if QSO redshifts are unrelated to their distances, there should be as many cases in which the foreground QSO has the *higher* redshift of the two. Thus, by using associated absorption to distinguish which of the two QSOs in a pair is in front of the other, we have a simple and straightforward test of the cosmological interpretation.

In all cases of associated absorption so far discovered, the foreground QSO has the lower redshift of the pair. *No* cases have been found in which the foreground QSO has the higher redshift. Application of statistical tests to the existing data (Shaver and Robertson, 1983, *Nature*, in preparation) already shows that the hypothesis that QSO redshifts are unrelated to distance is highly improbable.

Indeed, the mere existence of the phenomenon of associated absorption presents severe obstacles to non-cosmological interpretations of redshifts. The fact that several cases are now known establishes beyond doubt that these are not chance coincidences – the absorption is really associated with the foreground QSO. A non-cosmological (emission) redshift of that QSO would therefore require an identical non-cosmological origin for the absorption redshift – yet the absorption presumably arises in a region of quite different physical conditions.

This work can be expected to advance rapidly, as there are many published close pairs of QSOs still to be studied, and many more soon to emerge from the present objective prism

surveys. Much more definite conclusions regarding the cosmological interpretation of redshifts, the origin of heavy-element and Ly α absorption lines, and the relative incidence of common and associated absorption will soon be possible, and one may begin to explore statistically the sizes, cross-sections, and other properties of the absorbing regions.

PERSONNEL MOVEMENTS

STAFF

Arrivals

Europe

WOUTERS, Jacobus (NL), Designer/Draughtsman, 17.1.1983.
 DUCHATEAU, Michel (F), Electronics Technician, 1.2.1983.
 MAZZARIOL, Severino (I), Electronics Technician 1.2.1983.
 MARGUTTI, Pietro (I), Programmer, 14.2.1983.
 SCHENCK, Gloria (F), Receptionist, 1.3.1983.
 LUND, Glenn (New Zealander), Engineer/Physicist, 16.3.1983.

Chile

ALLAERT, Eric (B), Systems Analyst/Programmer, 1.3.1983.
 ANDREONI, Gaetano (I), Scientific Programmer, 1.3.1983.

Departures

Chile

VAN DEN BRENK, John (Australian), Electronics Technician, 4.3.1983.

FELLOWS

Departures

Europe

WALDTHAUSEN, Harald (D), 11.3.1983.

ASSOCIATES

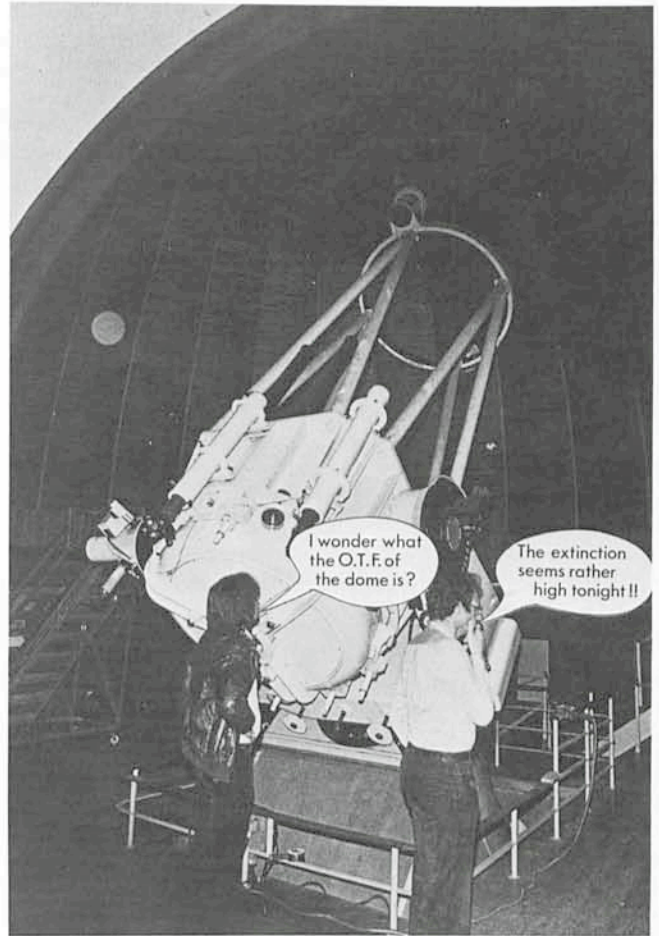
Departures

Europe

CHOUDRY, Amar (USA), 28.2.1983.

Chile

KOORNNEEF, Jan (NL), 31.3.1983.



When engineers observe by themselves! R. Wilson and B. Delabre at the 1.37 m at Merate. Photo O. Citterio.

COOPERANTS

Arrivals

Chile

GONDOIN, Philippe (F), 11.2.1983.

Departures

Chile

DUFLOT, Jean-Christophe (F), 31.1.1983.

ALGUNOS RESUMENES

Llegó a La Silla el telescopio de 2.2 m

El día 19 de enero arribó a Valparaíso el telescopio de 2.2 m a bordo del mercante chileno "Maule". El instrumento fabricado por Zeiss, fue embarcado en el puerto alemán de Bremen. Fue embalado en 46 cajones con un peso total de 112 toneladas. La descarga comenzó de inmediato y duró la noche entera. Al próximo día fueron cargados todos los cajones en 5 camiones que los llevaron a La Silla. El día 21 de enero se descargó el último cajón y todos ellos fueron colocadas en los lugares previstos. Se abrió el cajón que contenía el espejo principal para examinarlo. El espejo se encontraba en perfecto estado.

El montaje del telescopio comenzó el 14 de febrero y se espera que concluirá en julio.

Fibras ópticas en ESO

Durante observaciones experimentales hechas en noviembre de 1982 se llevaron a cabo algunos tests con fibras ópticas en el telescopio de 3.6 m. Para uno de los tests se interconectaron por fibras el foco primario del 3.6 m y el Espectrógrafo Coudé Echelle. Para ese propósito se prepararon tres cables de fibras ópticas, con un largo aproximado de 38 m cada uno y diámetros interiores de 85, 100 y 125 μ .

ESO, the European Southern Observatory, was created in 1962 to . . . establish and operate an astronomical observatory in the southern hemisphere, equipped with powerful instruments, with the aim of furthering and organizing collaboration in astronomy . . . It is supported by eight countries: Belgium, Denmark, France, the Federal Republic of Germany, Italy, the Netherlands, Sweden and Switzerland. It operates the La Silla observatory in the Atacama desert, 600 km north of Santiago de Chile, at 2,400 m altitude, where twelve telescopes with apertures up to 3.6 m are presently in operation. The astronomical observations on La Silla are carried out by visiting astronomers – mainly from the member countries – and, to some extent, by ESO staff astronomers, often in collaboration with the former. The ESO Headquarters in Europe are located in Garching, near Munich. ESO has about 120 international staff members in Europe and Chile and about 120 local staff members in Santiago and on La Silla. In addition, there are a number of fellows and scientific associates.

The ESO MESSENGER is published four times a year: in March, June, September and December. It is distributed free to ESO personnel and others interested in astronomy.

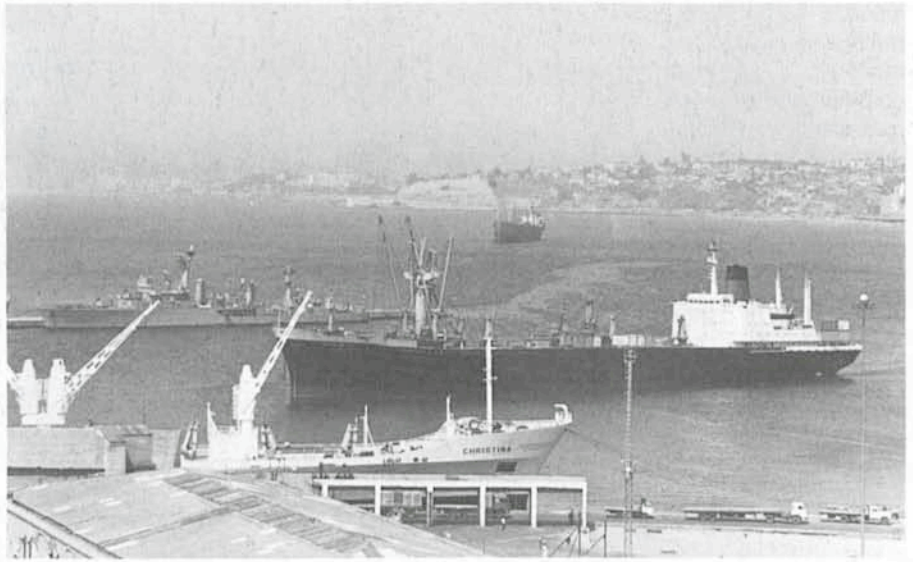
The text of any article may be reprinted if credit is given to ESO. Copies of most illustrations are available to editors without charge.

Editor: Philippe Véron
 Technical editor: Kurt Kjær

EUROPEAN
 SOUTHERN OBSERVATORY
 Karl-Schwarzschild-Str. 2
 D-8046 Garching b. München
 Fed. Rep. of Germany
 Tel. (089) 32006-0
 Telex 5-28282-0 eo d

Printed by Universitätsdruckerei
 Dr. C. Wolf & Sohn
 Heidemannstraße 166
 8000 München 45
 Fed. Rep. of Germany

ISSN 0722-6691



Llegada del mercante "Maule" a Valparaíso, con el telescopio de 2.2 m a bordo.

Los tests comprobaron que conexiones de fibras ópticas pueden ser usadas eficientemente en telescopios y se espera que las primeras conexiones ópticas completamente operables estarán listas para el uso regular de astrónomos en la primera mitad de 1984.

"136 Austria" observada en ESO

Hace algún tiempo el Dr. H. J. Schober de Austria hizo observaciones fotoeléctricas del asteroide 136 Austria. El asteroide descubierto en 1874 es un pequeño objeto con un diámetro de 41 kilómetros.

Las observaciones, llevadas a efecto durante cuatro noches en el telescopio de 61 cm de Bochum fueron bastante exitosas, y se pudo establecer un período de rotación de 11.5 horas.

El Dr. Schober piensa que como austríaco tuvo especial suerte de observar este asteroide en ESO, a pesar de que Austria aun no pertenece a la ESO como país miembro.

Contents

Latest News about the European Coordinating Facility for the Space Telescope . .	1
D. Enard and G. Lund: Fiber Optics at ESO. Part I: Coupling of the CES with the 3.6 m Telescope Using a 40 m Fiber Link	1
Tentative Time-table of Council Sessions and Committee Meetings in 1983	3
P. A. S. and D. K.: ESO Workshop on "Primordial Helium"	4
P. O. Lindblad, S. Jörsäter and A. Sandqvist: The Galaxy NGC 1365	5
P. Bouchet, M. Querci and F. Querci: Active Chromosphere in the Carbon Star TW Horologium	7
H. J. Schober: 136 Austria – Observed at ESO	11
Visiting Astronomers (April 1 – October 1, 1983)	12
S. Balon: Mechanics and the Stars	13
J. Isserstedt: Star Formation and Interstellar Matter in the Large Magellanic Cloud	14
List of Preprints Published at ESO Scientific Group	16
F. Rufener: The Telescope of Geneva Observatory and the Development of Geneva Photometry at La Silla	17
C. T. Hua and R. Louise: Morphological and Physical Study of Planetary Nebulae .	20
J. Andersen and B. Nordström: The Bright Star Catalogue Complete in Radial Velocities	22
P. Bouchet: Envelopes Around Carbon Stars	23
R. Foy: Chemical Composition in the Small Magellanic Cloud	24
K. Barse, P. Crane, P. Grosbøl, F. Middleburg, C. Ounnas, D. Ponz and H. Waldthausen: MIDAS – ESO's New Image Processing System	26
P. A. Shaver and J. G. Robertson: Absorption-Line Spectroscopy of Close Pairs of QSOs	28
Personnel Movements	31
Algunos Resúmenes	31